2010

Modeling and analysis of radial flux toroidally wound twin rotor permanent magnet motor

Ravi Kishore Pratapa
Louisiana State University and Agricultural and Mechanical College, kishore.pratapa@gmail.com

MODELING AND ANALYSIS OF RADIAL FLUX TOROIDALLY WOUND TWIN ROTOR PERMANENT MAGNET MOTOR

A Thesis

Submitted to the Graduate Faculty of the
Louisiana State University and
Agricultural and Mechanical College
in partial fulfillment of the
requirements for the degree of
Master of Science in Electrical Engineering
in
The Department of Electrical and Computer Engineering

by
Ravi Kishore Pratapa
Bachelor of Engineering, Anna University, 2005
May 2010

Dedicated to my family

ACKNOWLEDGEMENTS

First of all I would like to express my heartfelt and deepest appreciation to my advisor and major professor Prof. Ernest A. Mendrela for his invaluable suggestions and constant guidance. I also thank Prof. Leszek Czarnecki and Prof. Ashok Srivastava for sparing their time to be a part of my defense committee.

I would also thank Dr. Peter Chen, Dr. Arthur Shr and Dr. James Board for supporting me throughout my stay here at LSU.

I would like to express my gratitude towards my family members and my cousin Mrs.Lalitha Devarakonda for their support. Without their encouragement, my Masters would have been just a dream. I would also like to thank my friends Phani Mylavarapu, Manthan, Kalyana, Raghava, Sampath, Hemalatha, Shilpa, Srilakshmi and Ashwini who made my stay at LSU a pleasant memory.

TABLE OF CONTENTS

ACKNOWLEDGEMENTS iii

LIST OF TABLES vi

TABLE OF FIGURES vii

ABSTRACT ix

CHAPTER 1 INTRODUCTION 1
1.1 Literature Review on Twin-Rotor PM Motors 1
1.1.1 AFTWTRPM Motor 1
1.1.2 RFTWTRPM Motor 2
1.2 Objectives of the Thesis 3
1.3 Tasks to Be Done 4
1.4 Brief Description of Chapters 5

CHAPTER 2 RADIAL FLUX TOROIDALLY WOUND TWIN ROTOR PERMANENT MAGNET MOTOR 6
2.1 General Description 6
2.2 Principle of Operation 8
2.3 Motor Design Parameters 9

CHAPTER 3 DETERMINATION OF ELECTROMECHANICAL PARAMETERS OF RFTWTRPM MOTOR 11
3.1 Modeling in FEMM 4.0 11
3.2 FEM Motor Model 13
3.2.1 Linear 2-D FEM Model 13
3.2.2 Cylindrical 2-D FEM Model 19
3.3 Stator Winding Parameters 20
3.3.1 Phase Resistance 20
3.3.2 Self Inductance 21
3.3.3 Mutual Inductance 22
3.3.4 Synchronous Inductance 22
3.4 Electromechanical Parameters 23
3.4.1 Electromagnetic Torque 23
3.4.2 Electromotive force 26
3.4.3 Voltage across Terminals 27
3.4.4 Torque vs. Power Angle Characteristics 27

CHAPTER 4 PERFORMANCE CHARACTERISTICS OF RFTWTRPM MOTOR OPERATING AS BRUSHLESS DC MOTOR 30
4.1 Comparison of Synchronous Motor and Brushless DC Motor 30
4.2 Schematic model of Brushless DC Motor 32
4.3 Equivalent circuit of Brushless DC Motor 33

4.4 Dynamic simulation of Brushless DC Motor 36
4.5 Performance of Brushless DC motor with Cogging Torque 38

CHAPTER 5 CONCLUSIONS 44

REFERENCES 45

APPENDIX-A: TORQUE CHARACTERISTICS OF RFTWTRPM MOTOR..……47

APPENDIX B: PERFORMANCE CHARACTERISTICS OF RFTWTRPM MOTOR OPERATING AS BRUSHLESS DC MOTOR……49

APPENDIX-C: PERFORMANCE CHARACTERISTICS OF RFTWTRPM MOTOR OPERATING AS BRUSHLESS DC MOTOR IN STEADY STATE…….....50

VITA ...……..……...…….……51

LIST OF TABLES

Table 2.1 Specifications of RFTWTRPM motor.....10

Table 3.1 Final dimensions of rotor yoke and stator core in the linear model of the internal part.....16

Table 3.2 Final dimensions of rotor yoke and stator core in the linear model of the external part.....17

LIST OF FIGURES

Fig 1.1 Schematic diagram of AFTWTRPM motor 2

Fig 1.2 Principle of operation of AFTWTRPM motor 2

Fig 1.3 Transformation of AFTWTRPM motor into RFTWTRPM motor 3

Fig 2.1 Three dimensional cross-sectional view of RFTWTRPM motor 6

Fig 2.2 Cross-sectional scheme of RFTWTRPM motor 7

Fig 2.3 Gramme's three phase winding 7

Fig 2.4 Orientation of magnetic field in rotors 8

Fig 2.5 Cross-sectional view of RFTWTRPM motor 9

Fig 3.1 Angular displacement of poles in cylindrical RFTWTRPM motor 14

Fig 3.2 Linear model of the internal part derived from cylindrical model 15

Fig 3.3 Linear model of the internal part in FEMM model 16

Fig 3.4 Linear model of the external part derived from cylindrical model.....16

Fig 3.5 Linear model of the external part in FEMM model.....17

Fig 3.6 Phasor diagram of three phase currents 18

Fig 3.7 Flux density plot of linear internal part in FEMM 18

Fig 3.8 Flux density plot of linear external part in FEMM.....19

Fig 3.9 Cylindrical model of RFTWTRPM motor 20

Fig 3.10 Flux density plot of cylindrical model.....20

Fig 3.11 Scheme of the stator winding coil 21

Fig 3.12 Torque for single phase supply.....24

Fig 3.13 Torque for three phase supply 25

Fig 3.14 Cogging torque and synchronous torque waveforms 26

Fig 3.15 Equivalent circuit of the synchronous motor.....27

Fig 3.16 Synchronous motor operation.....28

Fig 3.17 Phasor diagram of the synchronous motor 28

Fig 3.18 Torque vs. power angle characteristics.....29

Fig 4.1 Circuit scheme of synchronous motor 31

Fig 4.2 Circuit scheme of brushless DC motor.....31

Fig 4.3 Schematic diagram of brushless DC motor 32

Fig 4.4 Equivalent circuit of brushless DC motor 33

Fig 4.5 Schematic representation of equation 3.1 34

Fig 4.6a SIMULINK block diagram of brushless DC motor.....39

Fig 4.6b SIMULINK block diagram of brushless DC motor subsystem.....40

Fig 4.7 Phase voltage and phase current waveforms in steady state 40

Fig 4.8 Dynamic characteristics of electromagnetic torque, speed and load torque vs. time.....41

Fig 4.9 Dynamic characteristics of load torque and source current waveform 41

Fig 4.10 Electromechanical characteristics in steady state.....41

Fig 4.11 Block diagram of brushless DC motor with cogging torque 42

Fig 4.12 Speed torque characteristics 43

ABSTRACT

The main objective of current thesis is the study of Radial Flux Twin Rotor Permanent Magnet (RFTWTRPM) motor. The tasks were to review the literature about RFTWTPM motors and model the motor using Finite Element Method Magnetics (FEMM 4.0). Later the performance of RFTWTRPM motor as a brushless dc motor was analyzed by using MATLAB/SIMULINK package.

To find the electrical and mechanical parameters of the RFTWTRPM motor, the rotor and stator dimensions of the motor were firstly optimized using linear FEMM model of the motor. The optimized dimensions were used to construct the cylindrical FEMM model. This model was later used to determine electrical and mechanical parameters.

The electro-mechanical parameters were used in the construction of motor block diagram in SIMULINK. This block diagram was used to test the performance of the motor as Brushless DC motor was analyzed for various dynamic and steady state conditions. It was observed that the RFTWTRPM motor was highly suitable to operate as Brushless DC motor.

CHAPTER 1

INTRODUCTION

Permanent Magnet Synchronous Motors (PMSMs) are widely used as electric drives in industries today. Attractive features of these motors like precise speed regulation, improved power factor and absence of slip makes them popular in the industrial world. The research carried out for several decades to increase the torque density and motor efficiency has lead to invention of several newer structures of PMSMs. Toroidally Wound Twin Rotor Permanent Magnet (TWTRPM) motor is one of these new structures [1].

1.1 Literature Review on Twin-Rotor PM Motors

Several new topologies of the Toroidally Wound Twin Rotor Permanent Magnet (TWTRPM) motors have been proposed. Some of these topologies are limited to low speed applications. As far as the motor geometry is concerned, the Twin-Rotor Permanent-Magnet motors can be classified into two types:

- Axial Flux Toroidally Wound Twin Rotor Permanent Magnet (AFTWTRPM) Motor.
- Radial Flux Toroidally Wound Twin Rotor Permanent Magnet (RFTWTRPM) Motor.

1.1.1 AFTWTRPM Motor

An AFTWTRPM motor shown schematically in fig 1.1 has a stator core placed in between two rotor discs. The stator consists of a laminated magnetic core which carries three- phase winding. Each of these rotor discs carries axially magnetized magnets which are mounted on its inner surface [3]. Therefore this arrangement results in two air gaps, each one of them placed in between the either sides of stator and magnetic poles. The twin rotor type of structure helps to improve performance of the motor by exposing higher percentage of stator surface during operation when compared to conventional motors. This process can be understood by looking at the principle of operation of this motor.

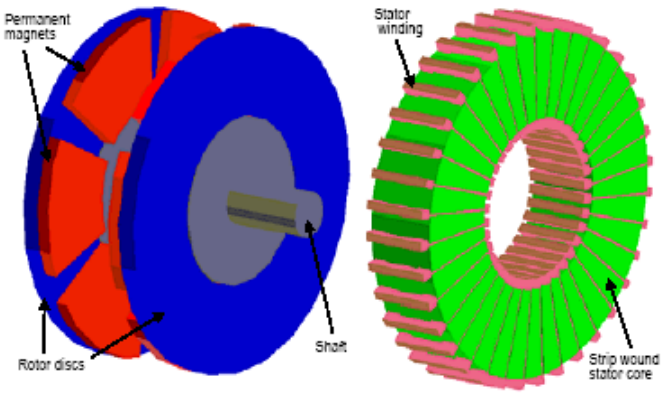

Fig 1.1 Schematic diagram of AFTWTRPM motor [8].

The general principle of operation is similar to that of two conventional machines in series. The magnets drive the flux on each side across the two air gaps into the stator. This flux then passes circumferentially through stator core, back across the air-gap and permanent magnets before travelling to the corresponding rotor discs (see Fig 1.2).

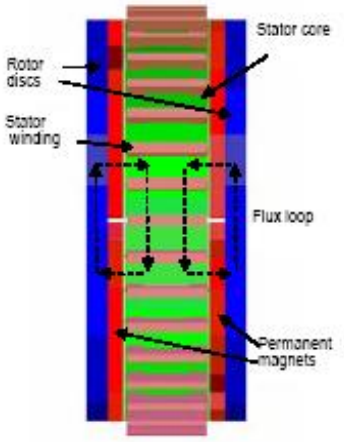

Fig 1.2 Principle of operation of AFTWTRPM motor [3].

The performance of Axial-flux motors is well documented in the literature positions [3], [4], [5] and [6].

1.1.2 RFTWTRPM motor

A RFTWTRPM motor can be regarded as a cylindrical version of an AFTWTRPM motor as shown in fig 1.3.

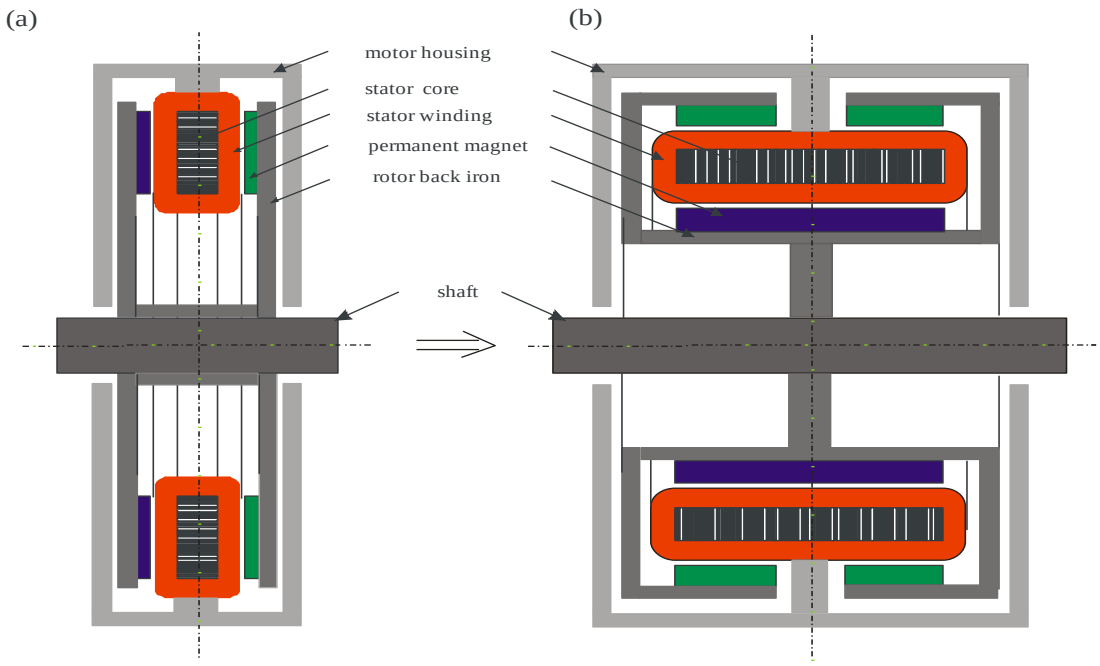

Fig 1.3 Transformation of AFTWTRPM motor into RFTWTRPM motor [12].

In this case the stator of AFTWTRPM motor has been expanded in axial direction and the rotor discs are transformed into cylinders with the permanent magnets facing the stator windings. The motor structure thus obtained consists of a cylindrical stator with Gramme's type of winding with inner and outer rotors. Unlike the case of AFTWTRPM motor where the magnetic flux crosses the air gap axially, the magnetic flux in the RFTWTRPM motor passes radially through both the air gaps. In general, with regard to stator structure, two versions of RFTWTRPM motors are available based on stator core. These motors can be classified as follows are:

i. RFTWTRPM motor with slot-less stator winding.

ii. RFTRWTPM motor with stator winding placed in slots.

A comparative study on the performances of slotted and slot-less versions of permanent magnet motors was done in [7]. There, it was observed that for the same amount of torque to be produced, slot-less motors need higher mmf compared to slotted motors. Owing to the supply of such high currents, these motors get heated up very fast and need special heat sinks for

dissipating the heat. This is the main advantage of using slotted motors instead of slot-less motors. Looking further into [8], it can be seen that in the slotted motors, RFTWTRPM motors have better cooling conditions because of the axial air gap than the AFTWTRPM motors with radial air gap. Additionally, RFTWTRPM motors have advantages of cheaper material cost and better chance of optimizing length to diameter. These features have encouraged a lot of research in favor of these motors. However, all the research carried out in this area discussed more about theoretical concepts and analysis ([1], [2] and [8]).Unfortunately, the dynamic analysis of these motors that could have helped researchers understand about the practical design of these models, was not carried out previously. Therefore the objective of this study is the design and dynamic analysis of a RFTWTRPM motor with slots.

1.2 Objectives of the Thesis

1. To determine the parameters of the equivalent motor model applying a 2-D Finite Element Method (FEM).
2. To determine the performance of the motor as Brushless DC motor using MATLAB/SIMULINK.

1.3 Tasks to Be Done

- Literature studies on synchronous motors with PM excitation, in particular the RFTWTRPM motors.
- Building of FEM motor model and simulation of magnetic field by using FEMM-4.0 software package.
- Determination of electromagnetic torque and motor equivalent circuit parameters of RFTWTRPM motor.
- Development of block diagrams in SIMULINK for simulation of dynamics of Brushless DC motor.

- Analysis of the motor performance under different supply and load conditions using MATLAB/SIMULINK model.

1.4 Brief Description of Chapters

Chapter 2 gives on a brief literature review on the RFTWTRPM motors. The details about current design model, its parameters and specifications are also discussed. Chapter 3 focuses on the FEM modeling of the RFTWTRPM motor. The parameters of the equivalent circuit of the motor and the torque developed by the motor are determined. Chapter 4 presents the modeling of the motor applying MATLAB/ SIMULINK. A detailed analysis of motor performance of motor under different supply and load conditions is given. In Chapter 5, the conclusions resulted from the motor performance analysis are presented.

CHAPTER 2

RADIAL FLUX TOROIDALLY WOUND TWIN ROTOR PERMANENT MAGNET MOTORS

The RFTWTRPM motors were proposed to improve machine density and torque. The structure, the principle of operation and the construction of the RFTWTRPM motor will be discussed in this chapter.

2.1 General Description

As explained in the introduction, the RFTWTRPM motor can be seen as a cylindrical transformation of AFTWTRPM motor. The stator in this case, is a cylinder placed between two rotor cylinders (Fig 2.1).

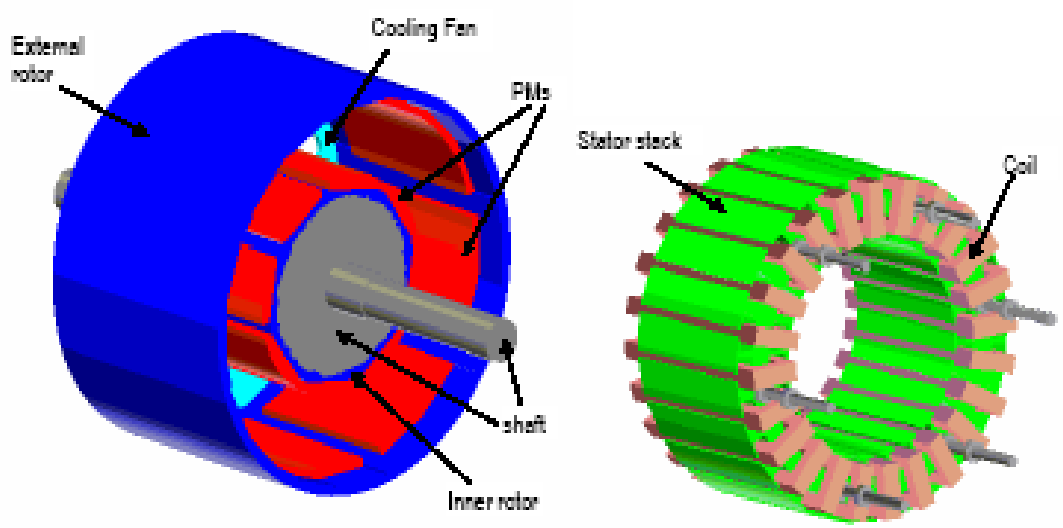

Fig 2.1 Three dimensional cross-sectional view of RFTWTRPM motor [8].

The stator core is a laminated structure with the slots on its inner and outer surface (see Fig 2.2). The laminations are necessary for stator to avoid eddy current losses. Since the stator for the present case is a dual sided stator, when excited, the magnetic field is produced in both inner and outer sides. This results in producing higher torque due to the rotor rotation.

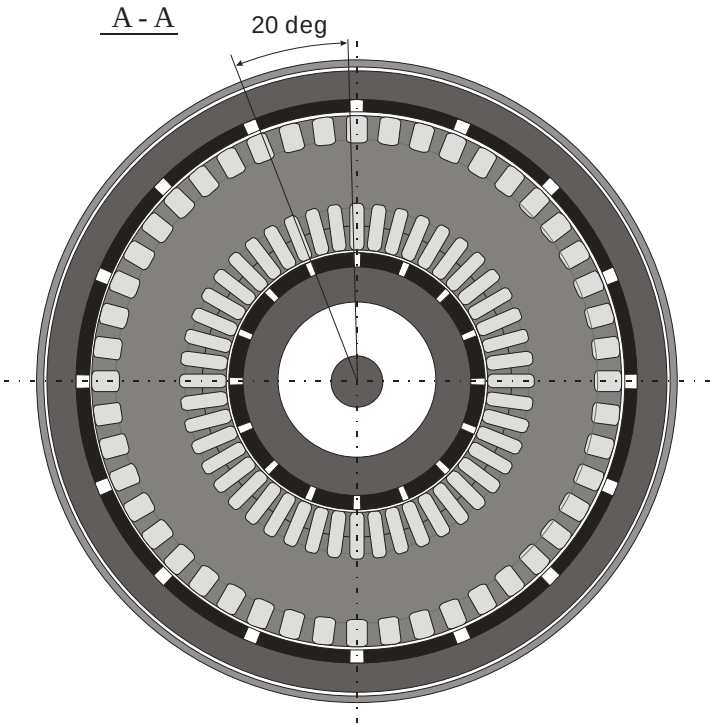

Fig 2.2 Cross-sectional scheme of RFTWTRPM motor

The coils are placed on the inner and outer slots. They may be connected in two-phase or any multi-phase system. In this thesis, a special type of three phase winding known as the Gramme's winding (Fig 2.3) has been considered for the design.

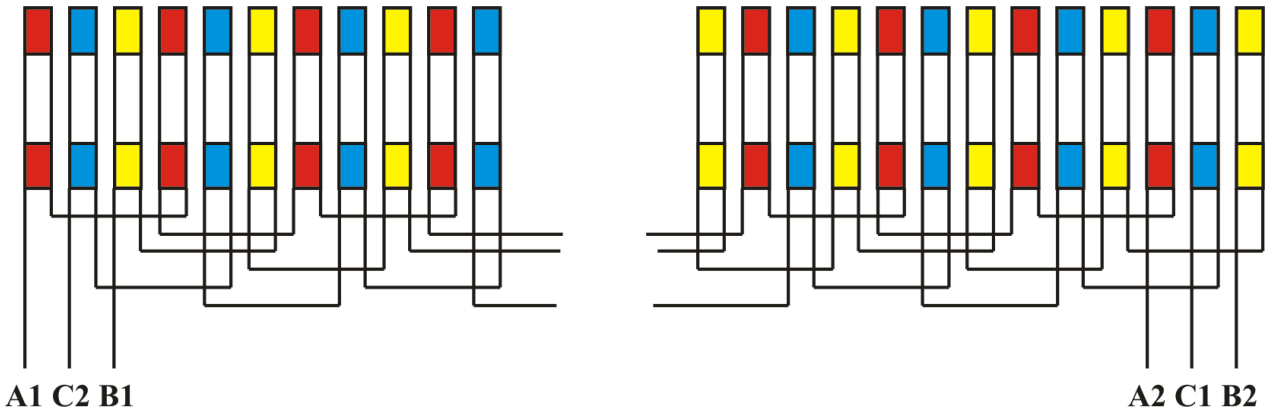

Fig 2.3 Gramme's three phase winding.

Gramme's type of winding has very short end connections comparing to overlap winding of conventional motors. Since the end connections are passive part of the winding, it does not contribute to the electromagnetic torque production. Hence the losses dissipated are much lesser

compared to those from the conventional windings. Therefore the efficiency of the motor with Gramme's type of winding is much more compared to the conventional windings.

The rotors in this type of motor are ferromagnetic cylinders with surface mounted permanent magnets. Since the magnetic field does not rotate with respect to the rotor cores, the rotor cylinders are made of solid iron. Contrary to the rotor, the magnetic field in stator is alternating.

The permanent magnets on the two rotor cylinders are polarized radially in the opposite directions. This makes the magnetic field in the core oriented as shown in Fig 2.4. Since the magnetic field in the stator is oriented radially and circumferentially, the stator core has to be laminated axially.

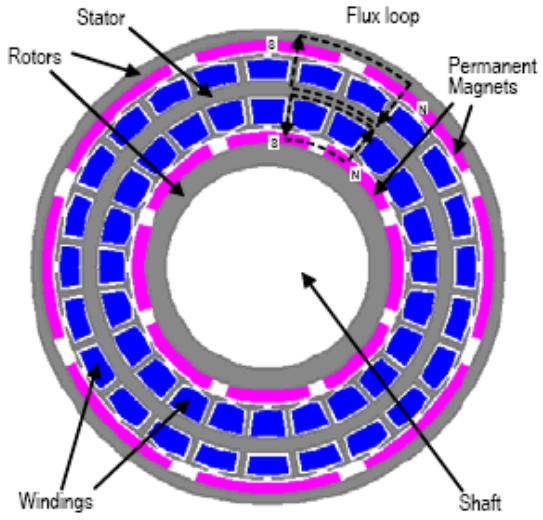

Fig 2.4 Orientation of magnetic field in rotors [8].

2.2 Principle of Operation

The principle of operation of this motor is similar to that of two PM three phase machines with rotors coupled. When a rotating magnetic field is produced in the stator windings, it forces the rotors to rotate along the field with synchronous speed. Depending on the load applied, the rotors develop some 'slip' while rotating synchronously along the rotating magnetic field.

2.3 Motor Design Parameters

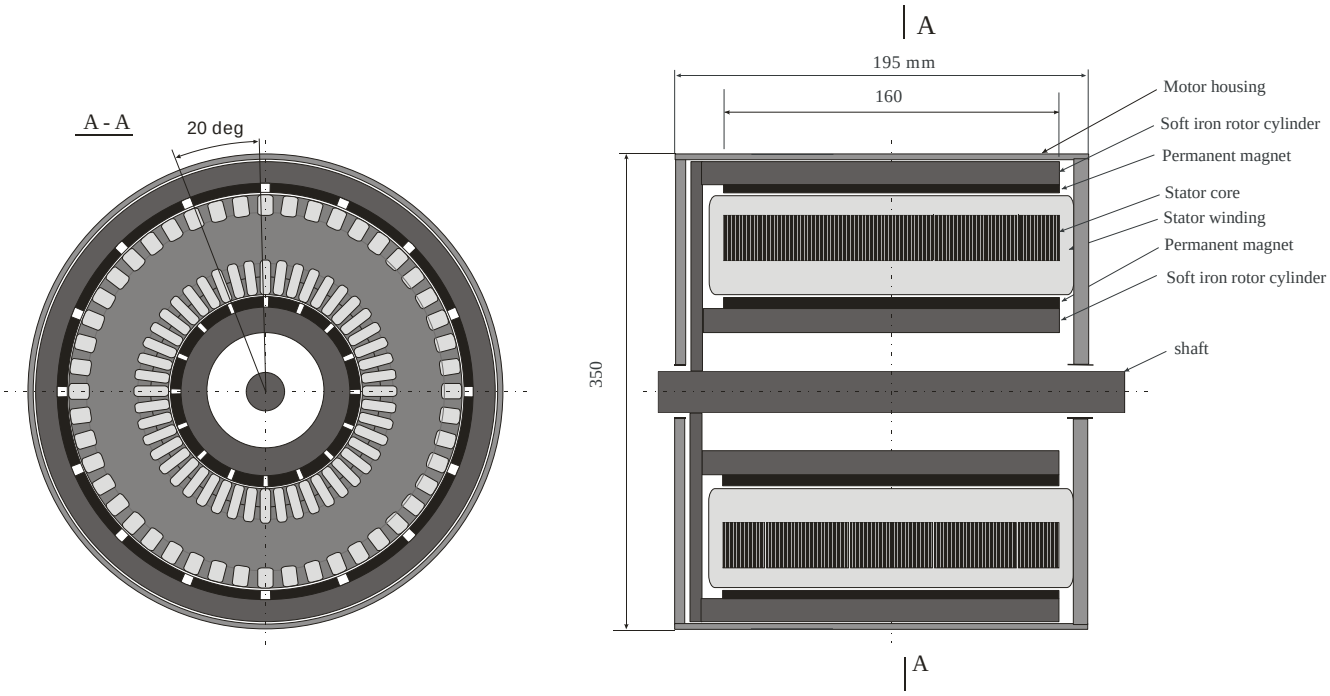

Fig 2.5 Cross-sectional view of the RFTWTRPM motor [11].

Fig 2.5 gives a clear description of the motor to be analyzed. The table 2.1 gives further details of the model to be constructed.

The very first objective of this thesis is to optimize the rotor core and stator yokes. These details will be discussed in Chapter-3.

Table2.1: Specifications of RFTWTRPM motor

Magnetic pole number	16
Winding:	
- Number of phases	3
- Number of coils/phase/pole	1
- Coil number	48
- Turn number/coil	10
- Wire diameter D_w	AWG9 – D_w=2.90575 mm
- Coil cross-section area A_c=14.4 X 8	112 mm^2
- Wire cross-section area A_w	6.63 mm^2
- $k_{Cu} = \frac{A_w \times N_w}{A_C} =$	2.84
Rotor speed	822 rpm (86.08 rad/s)
Permanent magnet:	
$H_C = 979kA/m,$ $\mu_r = 1.049,$ $B_r = \mu_r H_C \mu_o = 1.2905T$	
Magnet thickness	
Flux density in the rotor discs (permissible)	1.5 T
Flux density in the stator discs (permissible)	1.8 T
Rotor core	Steel 1117
Stator laminated core	US Steel type 2-S, 0.018 inch thickness

CHAPTER 3

DETERMINATION OF ELECTROMECHANICAL PARAMETERS OF RFTWTRPM MOTOR

To analyze motor performance, the motor equivalent circuit as well as the mechanical model will be used. To do this, the parameters of these two models should be determined first. Some of the parameters like winding resistance and moment of inertia of the rotor will be calculated by applying rather simple formulae. Other parameters like winding inductances and electromotive force constant K_E in the equation $E = K_E\ \omega_m$ will be determined by applying finite element method (FEM). This method will also allow finding the flux density distribution in the motor volume and electromagnetic torque developed by the motor. The particular program which will be used here is FEMM 4.0 [10].

3.1 Modeling in FEMM 4.0

Finite Element Method Magnetics (FEMM) 4.0 is a suite of programs used to solve low frequency electromagnetic problems on two dimensional planar and axi-symmetric domains [10]. An electromagnetic problem generally needs a lot of calculations for finding out various parameters associated with it. FEMM 4.0 simplifies this problem by reducing the calculations needed to find out parameters like flux density (B) and field intensity (H) by using Maxwell's equations.

Maxwell's equations are a set of differential equations used to describe the properties of electric and magnetic fields. FEMM uses two of these four equations. They are:

Ampere's law

$$\nabla \times H = J \tag{3.1}$$

where J is current density

H is field intensity

From Gauss' law for magnetism

$$\nabla \cdot B = 0 \tag{3.2}$$

where B is magnetic flux density

The quantities B and H can be related as follows

$$B = \mu H \tag{3.3}$$

where μ is magnetic permeability

For non-linear materials, the permeability is a function of B:

$$\mu = \frac{B}{H(B)} \tag{3.4}$$

The Magnetic Flux density can also be expressed in terms of magnetic vector potential (A) as

$$B = \nabla \times A \tag{3.5}$$

where A is magnetic vector potential

Using the above equations, Eq (3.5) can be written as follows:

$$\nabla \times \left(\frac{1}{\mu(B)} . \nabla \times A \right) = J \tag{3.6}$$

FEMM uses the form of Eq (3.6) to solve magneto-static problems with non-linear B-H relationship. Along these equations FEMM also uses a series of equations related to electric field distribution, electric field intensity (E) and electric flux density (D) in particular, are used to solve time-harmonic magnetic problems and electrostatic problems. These equations are used by Solvers part of FEMM for solving the problems. Explaining briefly, FEMM is divided into three parts:

a) Interactive shell (femm.exe)

This program is the interface to solve various types of problems in FEMM. It contains a CAD like interface for laying out the geometry of the problem to be solved and for defining material

properties and boundary conditions. Field solutions of these problems can be displayed in the form of contour and density plots. The program also allows the user to inspect the field at arbitrary points, as well as evaluate a number of different integrals and plot various quantities of interest along user-defined contours.

The interactive shell is integrated with Lua scripting language, which helps building and analyzing a geometry and evaluate the post-processing results.

b) Triangle (triangle.exe)

The triangle breaks down the solution region into various triangles.

c) Solvers (fkern.exe for magnetics and belasolv for electrostatics).

Each solver takes a set of data files that describe problem and solves the relevant Maxwell's equations to obtain values for the desired field throughout the solution domain. Therefore, each time a model is constructed in the FEM, the interactive shell, the triangle and the solvers co-ordinate together to get the desired field plots. In present case, the FEM model is used to modify the stator and rotor dimensions of RFTWTRPMM on the basis of flux density plots.

3.2 FEM Motor Model

Before the particular model of the motor will be used to find the flux density distribution and inductances, it is necessary to optimize the dimensions of stator and rotor yokes with respect to permissible flux densities in these two elements. To do this, the simplified linear FEM model will be used. Later, the cylindrical model will be developed.

3.2.1 Linear 2-D FEM Model

Optimizing the rotor and stator cores in the cylindrical model as such complicates the problem. Therefore by using the given design data, the cylindrical model is converted into linear motor. From Fig 3.1, it can be observed that the angular displacement of any two poles is $22.5°$. In order

to get the reliable results from linear motor model, the cylindrical structure was obtained using two parts:

a) Outer part containing outer stator winding, air gap and outer rotor.

b) Inner part containing inner stator winding, air gap and inner rotor.

Each of these parts was next developed into linear structure with respect to each air gap. The linear motor models are shown in fig 3.2 and fig 3.3. Since the cylindrical FEMM model is symmetrical, instead of converting the whole model as such, selective units of the model equal to the length of 2 pole pitches are developed into linear models. These linear models can be replicated, converted and integrated back to form the original cylindrical model.

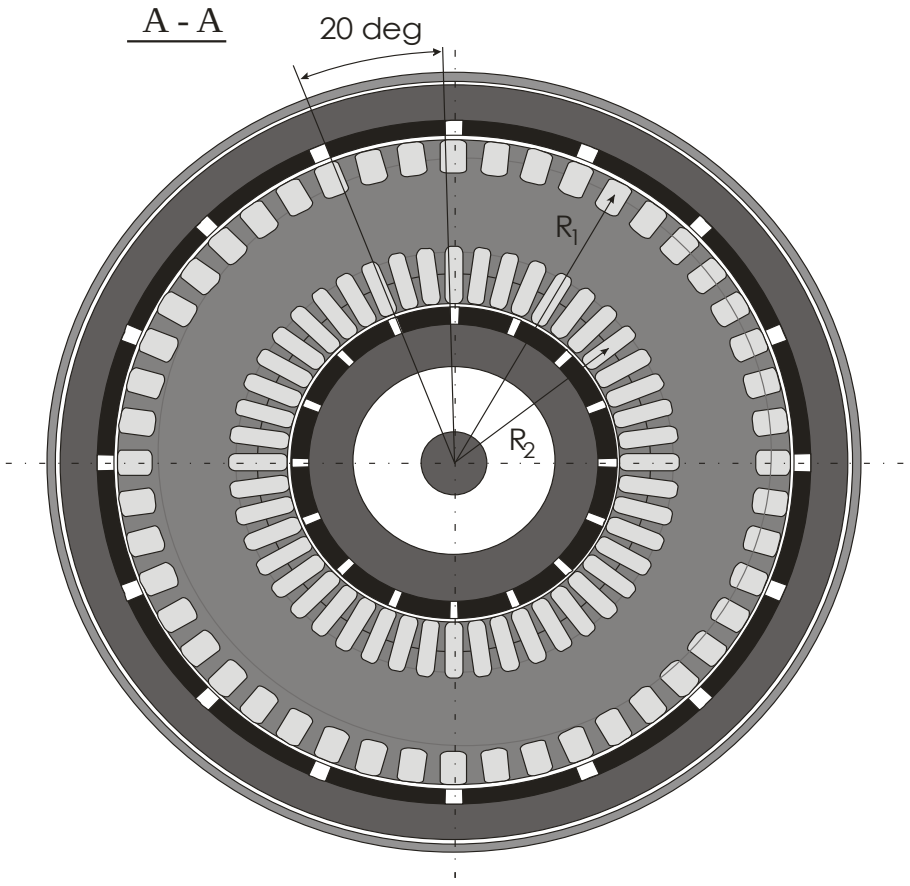

Fig 3.1 Angular displacement of poles in cylindrical RFTRWTRPM motor

The linear model of internal part shown in fig 3.2 was constructed by using these parameters. In this motor, the dimensions of rotor yoke and stator core were 11.5mm and 20mm respectively.

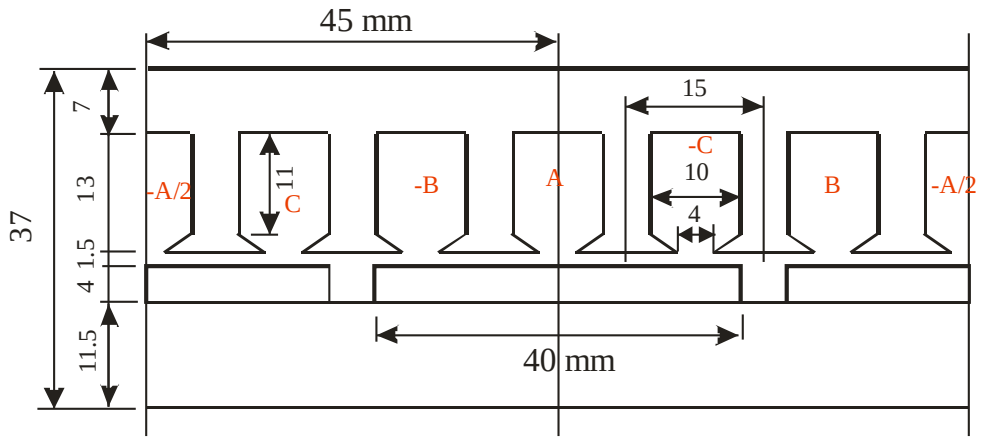

Fig 3.2 Linear model of internal part derived from cylindrical model

As mentioned previously, the aim of constructing this model is to observe the trend of flux density while varying the dimensions of rotor yoke until the flux density value reads as 1.5T. Similarly, the stator flux density should be obtained as 1.8T by varying stator dimensions, if necessary. It should be noted here that, the permissible value of flux density is higher in stator core than in the rotor because the stator core is made of laminated steel which goes into saturation at much higher values [12]. While varying the rotor and stator thicknesses, the desired values of flux densities were obtained at the dimensions shown in the Table 3-1. The linear internal motor model constructed in FEMM with the recorded dimensions can be seen in Fig 3.3.

Just like the internal rotor model, an external rotor linear model can be developed by converting cylindrical dimensions model of the external rotor, stator and windings with respect to their radii in the cylindrical model as shown in Fig 3.4. The dimensions of rotor and stator, thus derived were 17.5mm and 18mm respectively.

Table 3.1 Final dimensions of rotor core and stator yoke in the linear model of the internal part

Details	Before optimization	After optimization
The thickness of rotor core in internal part at which, the flux density was recorded as 1.5T	11.5 mm	10.5 mm
The thickness of stator yoke in internal part at which, the flux density was recorded as 1.8T	20 mm	20 mm

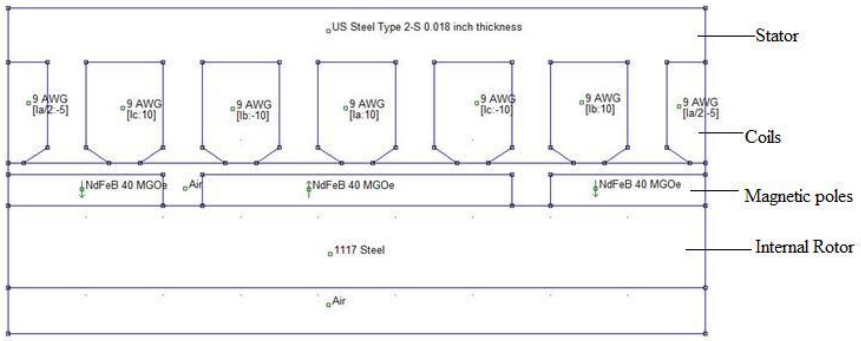

Fig 3.3 Linear model of internal part in FEMM model

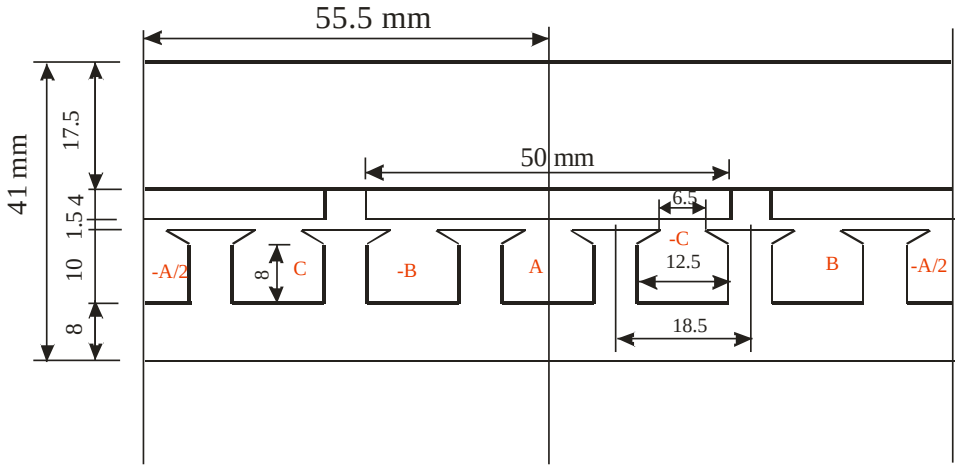

Fig 3.4 Linear model of external part derived from cylindrical model

As done in the linear model, the value of flux density in rotor core should be observed by varying the thickness of the rotor until the value reads 1.5T. The same procedure can be used to find the corrected dimensions of stator at Flux density of 1.8T. The recorded thickness values for the new external part can be seen in the Table 3.2.

Table 3.2 Final dimensions of rotor yoke and stator core in the linear model of the external part

Details	Before optimization	After optimization
The thickness of internal rotor core at which, the flux density was recorded as 1.5T	17.5 mm	12.5 mm
The thickness of internal rotor core at which, the flux density was recorded as 1.8T	18 mm	18 mm

The linear external motor model after optimization can be seen in Fig 3.5.

The flux density plots of the above two models can be observed from the FEMM, by applying three-phase currents.

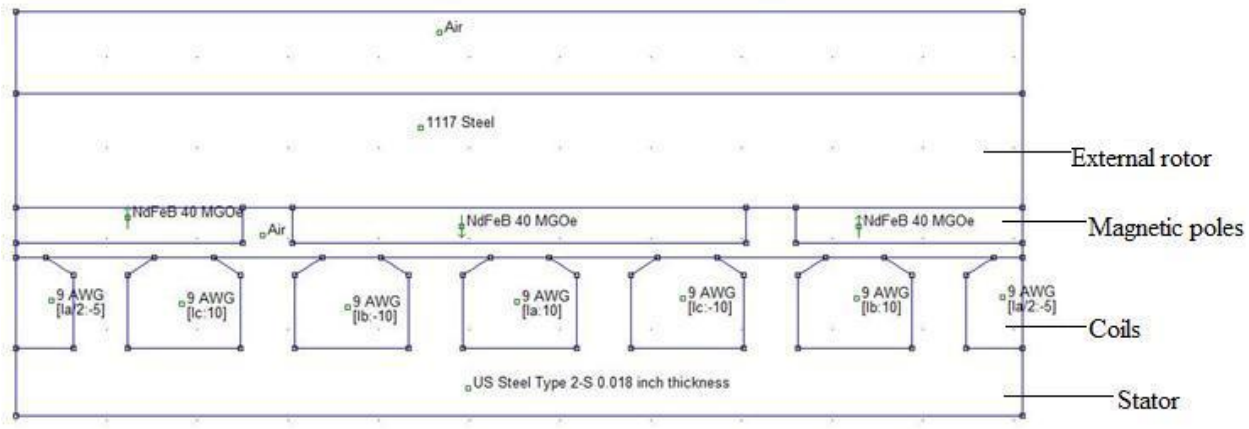

Fig 3.5 Linear model of external part in FEMM model

In the present case, the stator, the external and internal rotors from the above models were supplied with the following currents:

$$I_A = 35.5A;\ I_B = -17.75A;\ I_C = -17.75A;$$

The phasor diagram below in fig 3.5 depicts the three phase currents supplied to the current model.

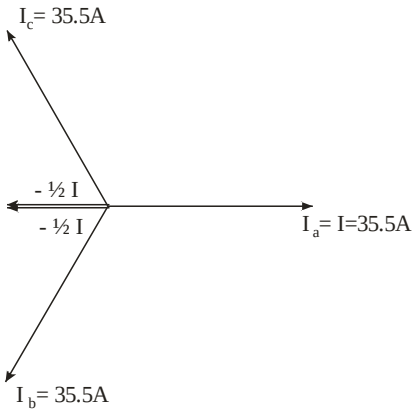

Fig 3.6 Phasor diagram of the three phase currents

The magnetic flux density plots for the linear models are shown in Fig 3.7 and Fig 3.8 respectively. The symmetrical distribution of magnetic field lines with respect to radial symmetrical axis of the magnets indicates a negligible effect of currents on resultant magnetic field.

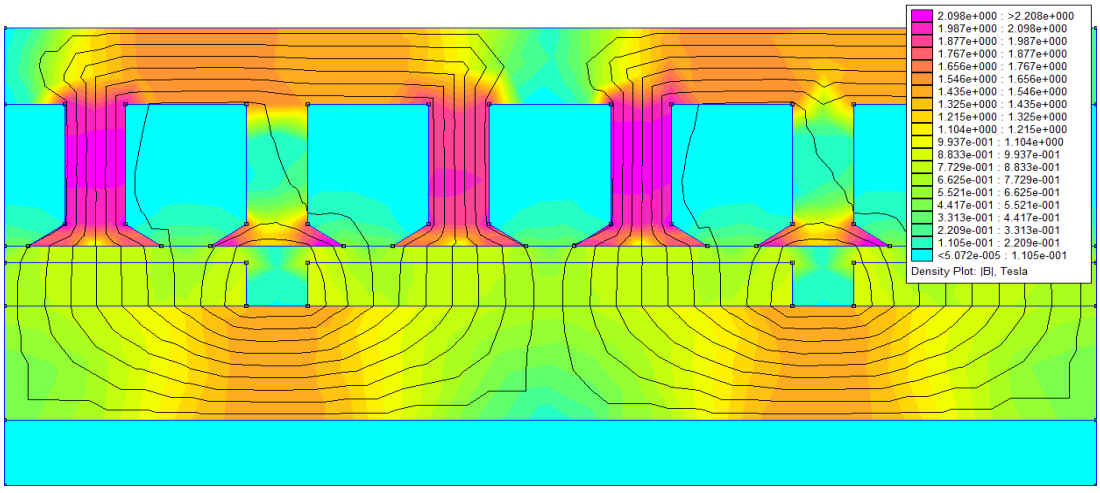

Fig 3.7 Flux density of linear internal part in FEMM

In both the plots, it can be observed that the magnetic field lines are symmetrical distributed with respect to the radial symmetrical axis of the magnets. This indicates a negligible influence of currents on resultant magnetic field. Now that the linear models have been corrected to attain the permissible flux density values, the next step is to integrate them back to form the cylindrical model.

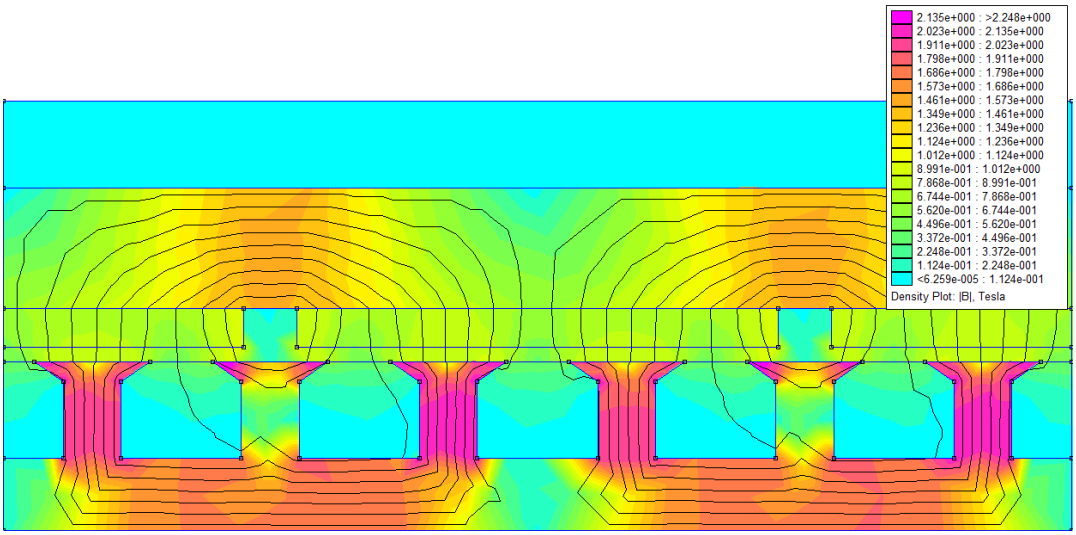

Fig 3.8 Flux density plot of linear external part in FEMM

3.2.2 Cylindrical 2-D FEM Motor Model

Since the linear models were derived using the angular displacement of each of the motor part and its radial distance from the centre, the cylindrical model of the RFTWTRPMM is developed simply by integrating the linear models of external and internal rotors. To do so, the rectangular co-ordinates from linear models are converted back into cylindrical co-ordinates by taking the radii R_1 and R_2 as reference. The cylindrical model, thus developed can be seen in Fig 3.9.

Since the cylindrical model is directly derived from the linear models, the flux densities of stator and both the rotors should be within permissible values. The stator core should have the flux density value of 1.8T, where as each of the rotors displays a flux density value of 1.5T. It can be recalled here that, since the stator is made of laminated steel, it goes into saturation at a relatively

higher value than rotor. The same can be observed by the flux density plot seen in Fig 3.10. The cylindrical FEM motor model created by using corrected stator and rotor dimensions of linear models is used to find out the stator winding parameters and electro-mechanical parameters.

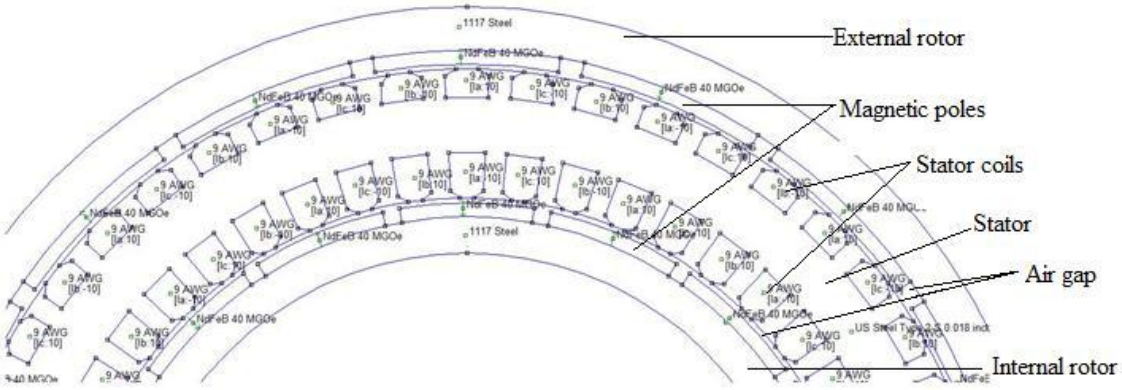

Fig 3.9 Cylindrical model of RFTWTRPM motor

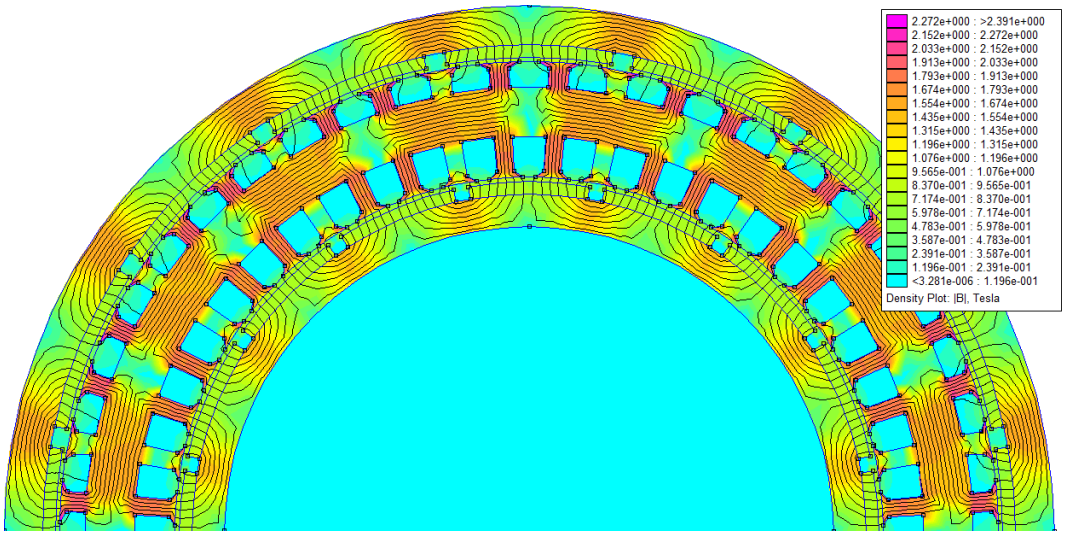

Fig 3.10 Flux density plot for cylindrical model

3.3 Stator Winding parameters

3.3.1 Phase Resistance

To calculate the phase resistance of the stator winding coil, the following figure will be used.

From Fig 3.11, the $L_{c,av}$ can be calculated as

$$L_{c,av} = 2(l_c + h_c) = 2(165 + 19) = 368\ mm \tag{3.7}$$

where l_c is 165mm

h_c is 19mm

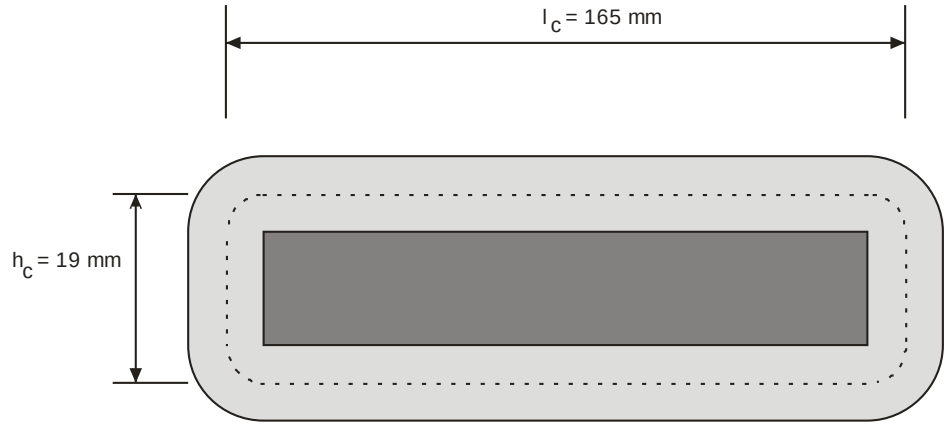

Fig 3.11 Scheme of the stator winding coil

The total length of the wire used for one phase is

$$L_{ph} = L_{c,av} \times N_c \times p = 0.368 \times 48 \times 16 = 282.62\ m \tag{3.8}$$

where N_c is the number of coils.

The phase resistance can be calculated as

$$R_{ph} = L_{ph} \times \frac{1}{A_w \times \gamma} = 282.62 \times \frac{1}{6.63 \times 10^{-6} \times 46.85 \times 10^{6}} = 0.9098\ \Omega \tag{3.9}$$

where A_w is the area of the windings

γ is the resistivity of the copper wire.

3.3.2 Self Inductance

The self inductance of each phase of the stator winding is calculated in the following steps:

i. The permanent magnets of the FEMM 4.0 model are turned into air.

ii. The current is assigned only to the phase whose self inductance is to be found.

iii. The FEMM 4.0 model is now analyzed with zero currents in the other phases and the flux/current value is noted down. This is the value of self inductance of the phase considered.

iv. The self inductance is calculated for all the three phases and the average of the values is considered the self inductance (L) of the cylindrical model.

The self inductance read from the FEMM 4.0 program for the cylindrical RFTWTRPMM is given as

$$L = \frac{(L_A + L_B + L_C)}{3} = 1.736 \text{ mH}. \tag{3.9}$$

3.3.3 Mutual Inductance

Calculating the mutual inductance for the cylindrical model is similar to that of calculating the self inductance.

i. Like the case of self inductance, the permanent magnets are turned to air for calculating mutual inductance.

ii. The mutual inductance between phase A and phase B is obtained by assigning current to phase A and retaining zero currents in phase B and phase C.

iii. The *flux linkage* value for phase B is found by analyzed the motor model. This value divided by the phase A current gives the mutual inductance, M_{AB} between phase A and phase B.

$$M_{AB} = \frac{flux\ linkage}{I_A} \tag{3.10}$$

iv. The mutual inductance is calculated for all the three phases and the average of the values is considered the mutual inductance (M) of the cylindrical model.

In present case the mutual inductance can be calculated using the formula

$$M = \frac{M_{AB} + M_{BC} + M_{CA}}{3} = 0.4661\ mH \tag{3.11}$$

3.3.4 Synchronous Inductance

The synchronous inductance L_S of the stator winding is defined as follows:

$$L_S = \frac{\lambda}{i} \tag{3.12}$$

where λ is the total flux linkage established by the currents in three phases

i is the phase current

The λ consists of flux generated by current i of the considered phase and fluxes established by other two phases. As a result, the synchronous inductance is expressed by the following equation

$$L_S = L + M = 2.202\ mH \tag{3.13}$$

where L is self inductance

M is mutual inductance

3.4 Electromechanical Parameters

To obtain the Equivalent circuit of the motor various electromechanical parameters are to be determined.

3.4.1 Electromagnetic Torque

The electromagnetic torque of the motor is directly proportional to flux density B and current I which are the functions of space angle [12]. This can be seen from the equation below

$$T_{em} = K_T B(\theta) \times i(\theta) \tag{3.14}$$

Since the distribution of magnetic flux and current along the stator periphery varies if the single phase is supplied the torque developed by the motor will vary too if the rotor would change its position with respect to stator.

This will be verified by using four cases:

i. Torque when only single phase is supplied

Phase A is supplied by the constant current of 35.5A, while the currents in phases B and C are equal to zero. Starting from angle $\theta = 0°$, the rotor position is varied for fixed intervals till 180° of electric angle with respect to stator. Using the FEMM model, the torque via weighted stress tensor is noted down for each interval. By plotting the torque with respect to position, the following characteristics are obtained as shown in Fig 3.12.

ii. Torque when three-phases are supplied

Phase A is supplied by the constant current of i_A =35.5A, while the current in phase B is i_A =17.75A and current in phase C is i_A =17.75A.

Similar to the previous case, the rotor position is varied for fixed intervals from angle $\theta = 0°$ till 360° of electrical angle θ_e with respect to stator. Using the FEMM model, the torque via weighted stress tensor is noted down. By plotting the torque with respect to position expressed by mechanical angle ($\theta = \frac{p}{2} \times \theta_e$), the characteristics shown in Fig 3.13 are obtained.

iii. Sinusoidal currents supply

Phases A, B and C are supplied by the three phase sinusoidal currents and the rotor flux B_R, displaced by 90° with respect to the current space vector I_S, moves synchronously as B_R.

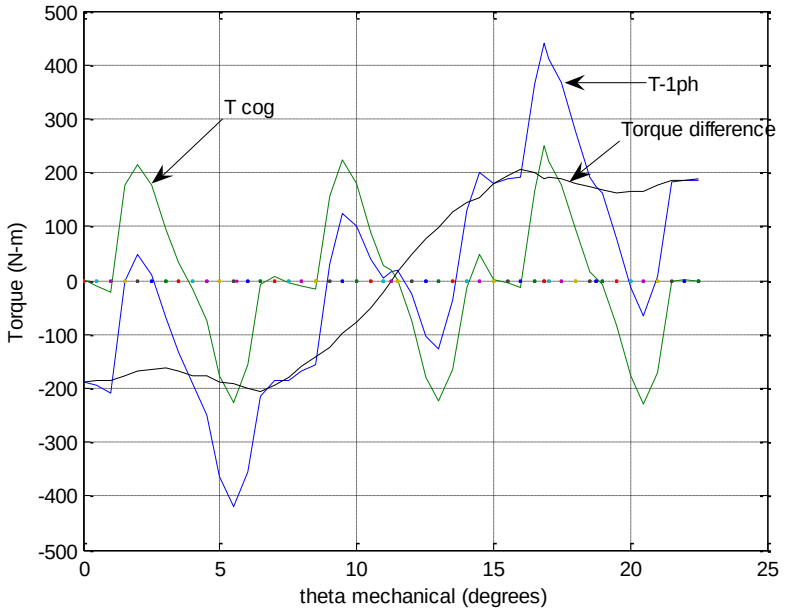

Fig 3.12 Torque for single phase supply

iv. The three phase winding is not supplied

Consider the case where three phases are not supplied with current. If the torque is now recorded by following the procedure used in previous cases, i.e. by varying the rotor position in fixed

intervals from 0° to 180° of electric angle with respect to stator. By plotting a waveform using the values obtained, the characteristics of cogging torque are obtained as shown in Fig 3.14. Cogging torque is caused due to the interaction between the permanent magnets of the rotor and the stator slots. In present thesis, the electromagnetic torque(T_{em}) was obtained by using the following formulae.

For the case-*i* (when current is supplied to a single phase)

$$T_{em} = T_{1-ph} - T_{cog} \tag{3.15}$$

where T_{1-ph} is single phase torque

T_{cog} is cogging torque

Similarly for case-*ii* (when current is supplied to three phases)

$$T_{em} = T_{3-ph} - T_{cog} \tag{3.16}$$

where T_{3-ph} is single phase torque

The distortions caused by cogging torque can be observed for single phase supply condition, three phase supply condition and synchronous torque condition (see Fig 3.12, Fig 3.13 and Fig 3.14).

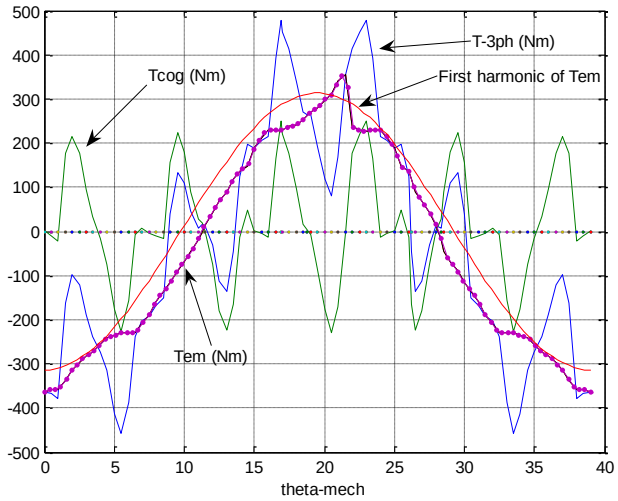

Fig 3.13 Torque for three phase supply

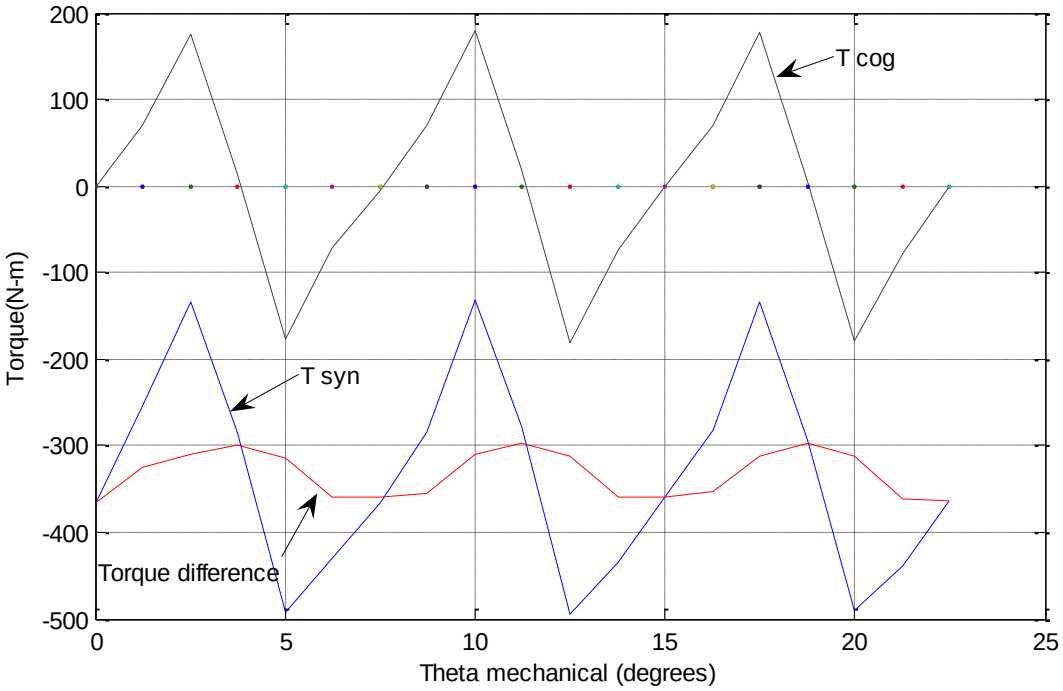

Fig 3.14 Cogging torque and synchronous torque waveform

3.4.2. Electromotive Force

When the rotor rotates with respect to the stationary stator, an electromotive force is induced in the stator winding by the magnetic flux. Thus, the peak value of emf in each phase, is given by the following equation:

$$E_{ph} = \omega_m \times K_E = 86.08 \times 6.858 = 590.305\ V \tag{3.17}$$

where ω_m is the rotor speed in radians per second

K_E is the co-efficient that can be calculated as follows [14]

$$\text{Since } K_E = \frac{2}{3} \times \frac{T_{em}}{I_A} = 6.858 \tag{3.18}$$

3.4.3. Voltage across Terminals

If the machine operates as synchronous motor, the voltage of the motor can be calculated using the equivalent circuit as shown in Fig 3.15.

The rms phase voltage can be calculated as

$$V_{ph} = E_{ph} + RI_A + jX_S I_A \tag{3.19}$$

$$= 590.305 + (0.281 \times 35.5) + j(2 \times \pi \times 60 \times 2.202 \times 10^{-3} \times 35.5)$$

$$= 599.98 + j\,29.48 = 600.7e^{j2.81}\ \text{V}$$

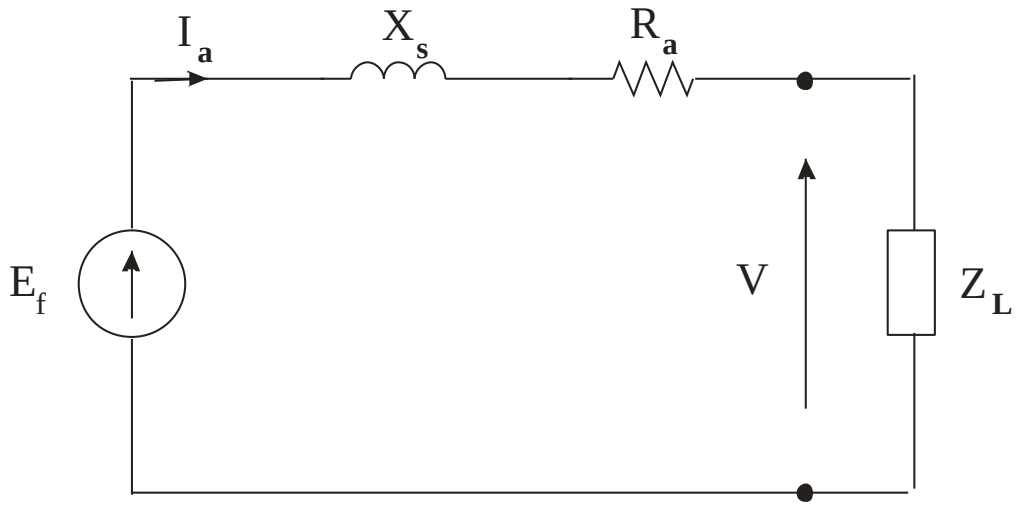

Fig 3.15 Equivalent circuit of the synchronous motor

where E_{ph} is the phase emf induced in a stator winding

RI_A is the voltage drop across the resistance winding

$jX_S I_A$ is the voltage drop across the phase inductance

3.4.4 Torque vs. Power Angle Characteristics

When the 3-phase armature winding of the synchronous motor is connected to a 3-phase ac supply, the stator currents produce a rotating magnetic flux as in 3-phase induction machines. The magnetic flux of the PM's is steady with respect to the rotor. To produce torque, these two magnetic fluxes cannot move with respect to one another. This means that the rotor should rotate with the same speed as the rotating flux produced by the stator [14]. (see Fig 3.16)

When the machine operates as synchronous motor in steady state conditions, the electromagnetic power as a function of power angle δ (see Fig 3.16) can be calculated from the equation:

$$P_{em} = m \cdot Real(E_f \cdot I_a) \tag{3.20}$$

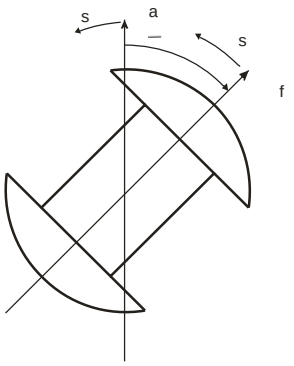

Fig 3.16 Synchronous motor operation

where $I_A = \frac{E_f - V_{ph}}{Z_s}$ and $E_f = |E_f| e^{j\delta}$

$$P_{em} = m \cdot \left(\frac{|V_{ph}||E_s|}{|Z_S|} \cos(\varphi_s - \delta) - \frac{|V_{ph}|^2}{|Z_S|} \cos(\varphi_s) \right) \tag{3.21}$$

In large synchronous machines ***Ra*** << ***Xs***, thus ***Zs*** = ***Xs*** and ***φs*** = ***90o***. Then the power can be assumed to be:

$$P_{em} = m. \left(\frac{|V_{ph}||E_s|}{|Z_S|} \sin(\delta) \right) \tag{3.22}$$

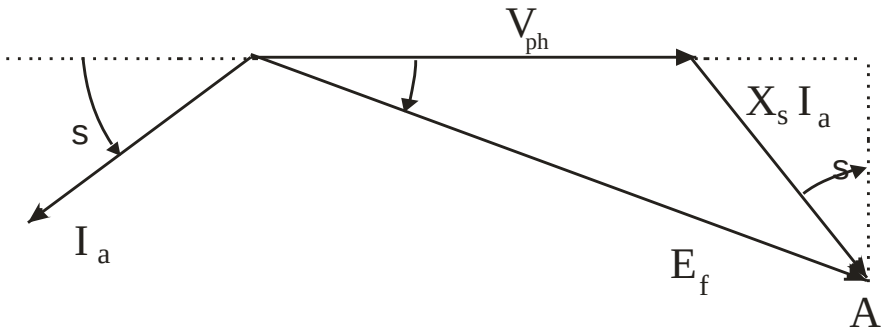

Fig 3.17 Phasor diagram of a synchronous motor

Since Torque can be written as:

$$T_{em} = \frac{P_{em}}{\omega_s} \tag{3.22}$$

On the basis of Eq 3.20 and Eq 3.21, the Torque-power angle characteristics were obtained as follows:

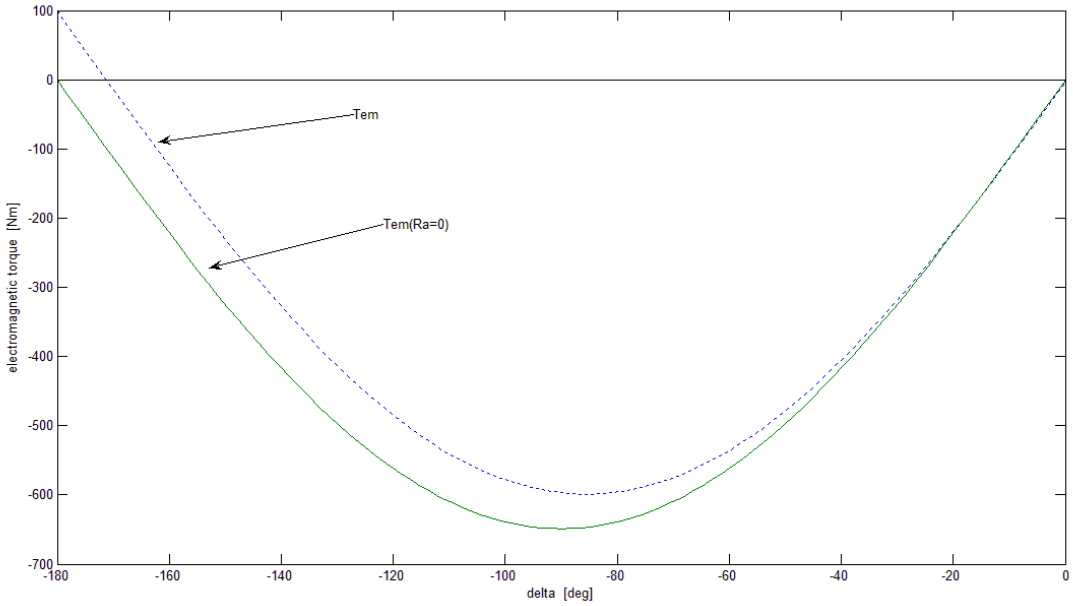

Fig 3.18 Torque vs. power angle characteristics

The performance of RFTWTRPM motor as a brushless DC motor will be discussed in Chapter-4.

CHAPTER 4

PERFORMANCE CHARACTERISTICS OF RFTWTRPM MOTOR OPERATING AS BRUSHLESS DC MOTOR

A three phase permanent magnet motor can be operated in two different modes of operation. They are:

- Synchronous motor
- Brushless DC motor.

Both these modes of operation use different control signal. While synchronous motors use an external controller for operation, the brushless dc motors use a signal from their corresponding rotor for operation. Therefore by using a rotor feedback position signal, a synchronous motor can operate as a brushless dc motor. In present chapter, the dynamic and steady state characteristics of the RFTWTRPM motor operating as a brushless dc motor are to be determined. For this purpose MATLAB/SIMULINK software is utilized.

4.1 Comparison of Synchronous Motor and Brushless DC Motor

The supply circuit scheme of a synchronous motor can be seen in Fig 4.1. The rotor of the synchronous motor rotates synchronously with the magnetic field generated by the stator winding. Due to very high inertia acting on the motor at the start, at start-up the rotor cannot instantaneously shoot to its synchronous speed. However, if the stator winding is supplied with frequency, the rotor speed gradually increases from 0 to its rated value. Hence, the motor has to be supplied from a variable frequency inverter [14]. The frequency can be controlled by imposing the desired reference frequency or the motor itself can set an appropriate frequency value required for its actual speed. On the contrary, the brushless dc motor is equipped with a speed or position sensor as shown in Fig 4.2. The motor operates with “self controlled frequency” using the sensor.

Looking at the construction of both these motors, some similarities can be found. For instance, in both the cases only the stator is wound. In both the cases, permanent magnets can be attached to the rotor surface or can be buried. Owing to these similarities in both types of motors, the synchronous motors can function as brushless DC motors in practical applications.

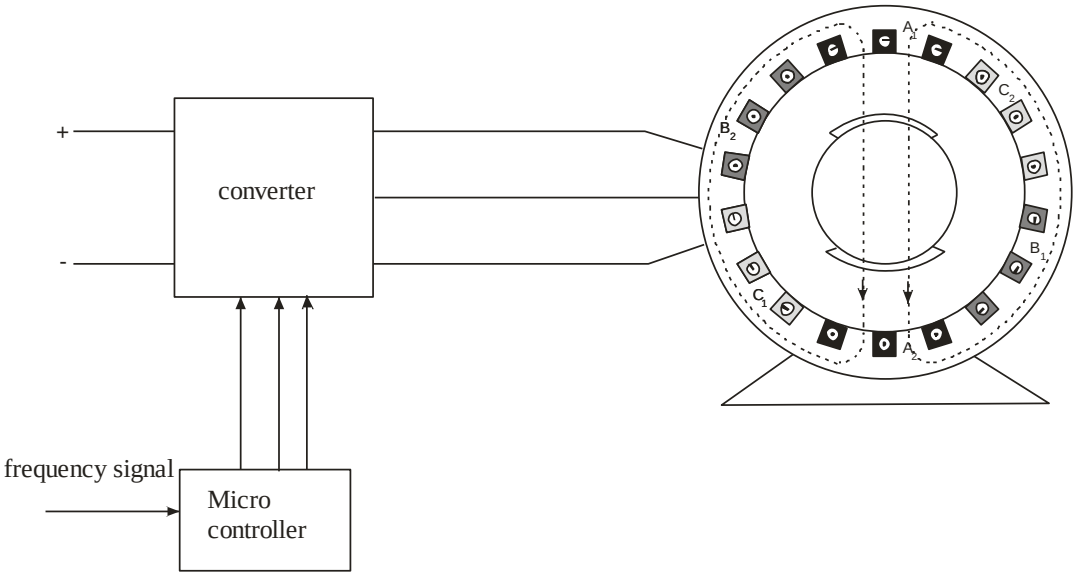

Fig 4.1 Circuit scheme of synchronous motor

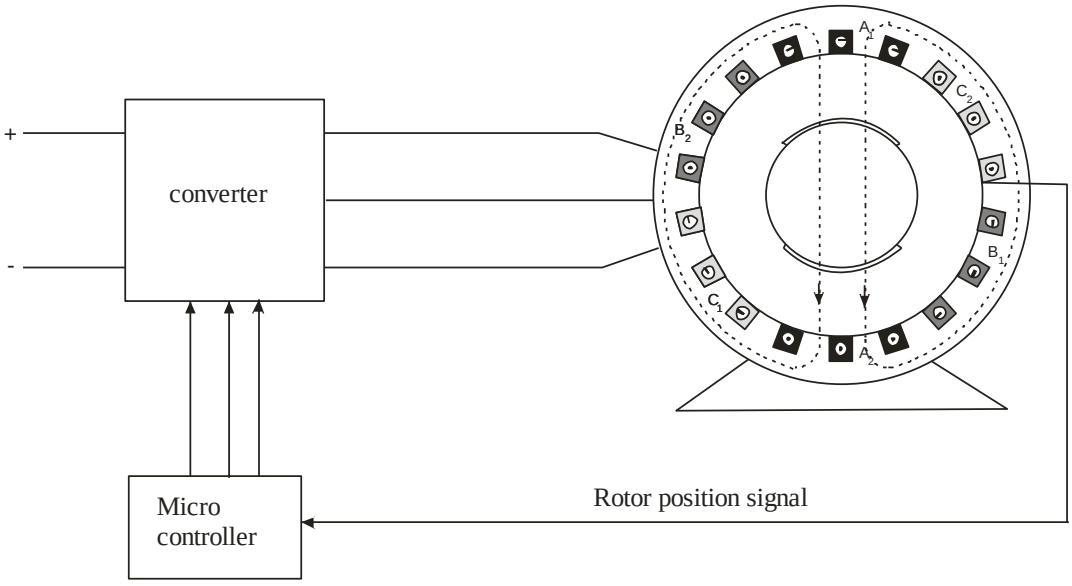

Fig 4.2 Circuit scheme of brushless DC motor

4.2 Schematic model of Brushless DC motor

The schematic diagram of a brushless DC motor is shown in fig 4.3. In brushless DC motor, the stator flux (Φ_s) rotates synchronously with rotor flux (Φ_f). This condition can be achieved by schematically switching the transistors connected to the motor. For example, in Fig 4.3, the transistors 1 and 6 are closed. This results in current supply to phases A and C. After $\omega t = 60°$, the phases A and B are supplied current, because their corresponding transistors switch on by the signal from position sensor.

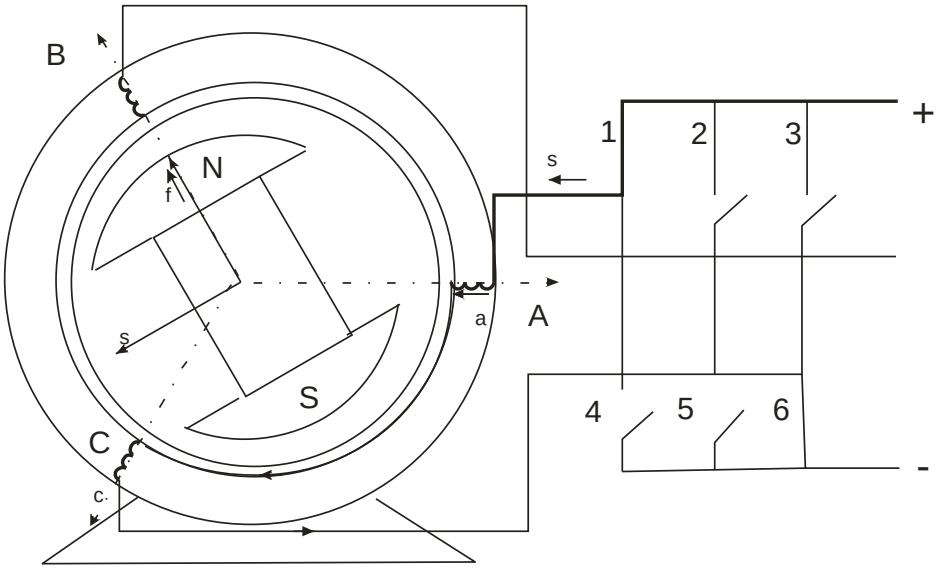

Fig 4.3 Schematic diagram of brushless DC motor

A position sensor should be applied to the motor, in order to supply the appropriate phase of the brushless dc motor. A signal from this sensor gives information to the controller about which phases should be supplied. The controller then switches these phases. It means the brushless DC motor operates with the position feedback loop as shown in fig 4.2. The frequency the three phases are supplied depends on the speed of the rotor. Hall sensors, optical sensors or induction sensors are used to sense the position of the rotor. The controller checks the position information and determines through simple logic which phase winding should be switched **ON** and switched **OFF**.

4.3 Equivalent circuit for Brushless DC Motor

The equivalent circuit of a brushless dc motor is shown in fig 4.4. It is assumed that the brushless dc motor is connected to the output of the inverter, while the inverter input terminals are connected to a constant supply voltage. The equivalent circuit model that refers to this circuit diagram is shown in Fig.4.1.

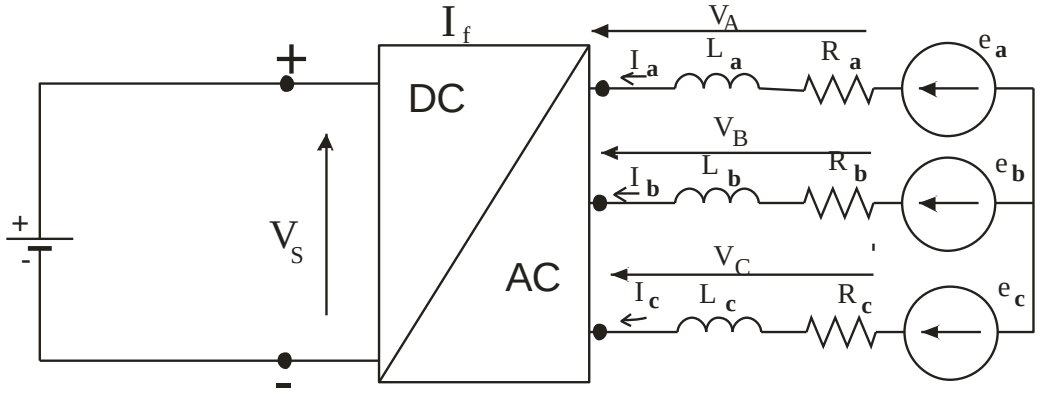

Fig 4.4 Equivalent circuit of brushless DC motor

While using the equivalent circuit model above for analysis, the following assumptions are made:

1. All the elements are linear and no core losses are considered.
2. EMF (e_a) and cogging torque vary sinusoidally with rotational angle θ_e
3. The 3-phase motor winding is connected in star.
4. Due to surface mounted permanent magnets, winding inductance is constant.
5. Voltage drops across diodes, transistors and connecting wire inductances are ignored.

The equations that govern this model are as follows.

$$V_A = V_N + V_{SA}$$
$$V_B = V_N + V_{SB} \quad (4.1)$$
$$V_C = V_N + V_{SC}$$

where v_{SA}, v_{SB}, v_{SC} are the inverter output voltages that supply the 3 – phase winding

v_A, v_B, v_C are the voltages across the motor armature winding

v_N – voltage at the neutral point.

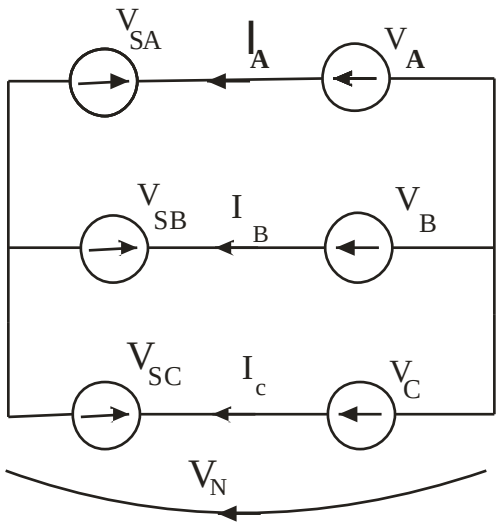

Fig. 4.5 Schematic representation of equation 3.1

Assuming a symmetrical winding and balanced system, the voltage equation across the motor winding can be written as follows:

$$\begin{bmatrix} V_A \\ V_B \\ V_C \end{bmatrix} = \begin{bmatrix} R_A & 0 & 0 \\ 0 & R_B & 0 \\ 0 & 0 & R_C \end{bmatrix} \begin{bmatrix} i_A \\ i_B \\ i_C \end{bmatrix} + \frac{d}{dt} \begin{bmatrix} L_A & M_{AB} & L_{AC} \\ L_{BA} & L_B & M_{BC} \\ M_{CA} & L_{CB} & L_C \end{bmatrix} \begin{bmatrix} i_A \\ i_B \\ i_C \end{bmatrix} + \begin{bmatrix} e_A \\ e_B \\ e_C \end{bmatrix} \tag{4.2}$$

These equations can also be represented in the matrix form as:

$$\boldsymbol{V_A} = \boldsymbol{R_A}\, \boldsymbol{I_A} + \frac{d}{dt} \boldsymbol{L_A} \cdot \boldsymbol{I_A} + \boldsymbol{E_A} \tag{4.3}$$

Since $R_A = R_B = R_C = R_A$, the resistance can be converted into the following vector form:

$$\boldsymbol{R_A} = \begin{bmatrix} R_A & 0 & 0 \\ 0 & R_A & 0 \\ 0 & 0 & R_A \end{bmatrix} \tag{4.4}$$

The self and mutual inductances are constant for surface mounted permanent magnets on the cylindrical rotor and the winding is symmetrical. Therefore

$L_A = L_B = L_C = L$ and $M_{AB} = M_{BC} = M_{CA} = M$

Using the above conditions, the inductance can be presented as:

$$\boldsymbol{L_A} = \begin{bmatrix} L & M & M \\ M & L & M \\ M & M & L \end{bmatrix} \tag{4.5}$$

Also, considering the Y-connected stator winding, the vector sum of currents in the three phases is zero.

$$i_A + i_B + i_C = 0 \tag{4.6}$$

Therefore, the voltage takes the following form:

$$\begin{bmatrix} V_A \\ V_B \\ V_C \end{bmatrix} = \begin{bmatrix} R_A & 0 & 0 \\ 0 & R_B & 0 \\ 0 & 0 & R_C \end{bmatrix} \begin{bmatrix} i_A \\ i_B \\ i_C \end{bmatrix} + \frac{d}{dt} \begin{bmatrix} L_S & 0 & 0 \\ 0 & L_S & 0 \\ 0 & 0 & L_S \end{bmatrix} \begin{bmatrix} i_A \\ i_B \\ i_C \end{bmatrix} + \begin{bmatrix} e_A \\ e_B \\ e_C \end{bmatrix} \tag{4.7}$$

where $L_S = L - M$

θ_e is the angle between a particular phase A and the rotor, at any given time. Choosing phase-A as the reference, the electromotive forces written in the form of a matrix, $\boldsymbol{E_A}$ can be written as follows:

$$\boldsymbol{E_A} = \frac{K_E}{P} \begin{bmatrix} sin\theta_e \\ \sin(\theta_e - \frac{2\pi}{3}) \\ \sin(\theta_e - \frac{4\pi}{3}) \end{bmatrix} \frac{d\theta_e}{dt} \tag{4.8}$$

Now, assuming $P_{in} = P_{out}$, the inverter input current can be written as:

$$i_{sk} = \frac{1}{r_S}(i_A v_{SA} + i_B v_{SB} + i_A v_{SC}) \tag{4.9}$$

The mechanical system shown schematically in Fig. 4.6 is defined by the following equations:

$$T_{em} = J_{eq} \frac{d\omega_m}{dt} + B\omega_m + T_L - T_{cog} \tag{4.10}$$

where $J_{eq} = J_M + J_L$. Here J_{eq} is the equivalent moment of inertia

J_M, J_L are moment or inertia of motor and load respectively

B is co-efficient of friction

T_L and T_{cog} are load torque and cogging torque respectively

The electromagnetic torque for this 3-phase motor is dependent on the current (*i*), speed (ω) and electromotive force (e). This relation can be represented as:

$$T_{em} = \frac{e_A i_A}{\omega_m} + \frac{e_B i_B}{\omega_m} + \frac{e_C i_C}{\omega_m} = K_E(f_a(\varphi_e).i_A + f_b(\varphi_e).i_B + f_c(\varphi_e).i_C \quad (4.11)$$

where $f_a(\varphi_e) = sin\theta_e$

$$f_b(\varphi_e) = \sin\ (\theta_e - \frac{2\pi}{3})$$

$$f_c(\varphi_e) = \sin\ (\theta_e - \frac{4\pi}{3})$$

Using all the equations above, the system in state space form can be given as:

$$\dot{x} = Ax+Bu \quad (4.12)$$

$$\boldsymbol{x} = [\, i_A \quad i_B \quad i_C \quad \omega_R \quad \theta_e \,]^t \quad (4.13)$$

$$\boldsymbol{A} = \begin{bmatrix} \frac{-R_S}{L_S} & 0 & 0 & \frac{-K_E(f_a(\varphi_e))}{L_S} & 0 \\ 0 & \frac{-R_S}{L_S} & 0 & \frac{-K_E(f_b(\varphi_e))}{L_S} & 0 \\ 0 & 0 & \frac{-R_S}{L_S} & \frac{-K_E(f_c(\varphi_e))}{L_S} & 0 \\ \frac{-K_E(f_a(\varphi_e))}{J} & \frac{-K_E(f_b(\varphi_e))}{J} & \frac{-K_E(f_c(\varphi_e))}{J} & \frac{-D}{J} & 0 \\ 0 & 0 & 0 & \frac{P}{2} & 0 \end{bmatrix} \quad (4.14)$$

$$\boldsymbol{B} = \begin{bmatrix} \frac{1}{L_S} & 0 & 0 & 0 \\ 0 & \frac{1}{L_S} & 0 & 0 \\ 0 & 0 & \frac{1}{L_S} & 0 \\ 0 & 0 & 0 & \frac{-1}{J} \\ 0 & 0 & 0 & 0 \end{bmatrix} \quad (4.15)$$

$$\boldsymbol{x} = [\, V_A \quad V_B \quad V_C \quad T_L \,]^t \quad (4.16)$$

4.4 Dynamic simulation of the Brushless DC Motor

The simulation of the brushless dc motor was done using the software package MATLAB/SIMULINK.

- **Data of the Drive System**

The SIMULINK block diagram of Brushless DC motor drive system system is shown in Fig. 4.1. This system is supplied from the battery of 400 V with the capacitor connected in parallel as shown. The data of these elements are as follows:

E_b = 400 V - EMF of the battery

R_S = 0.0005 Ω - source resistance

R_C = 10 Ω - resistance in series with capacitor

C = 0.00001 F - capacitance

The inverter is assumed to be ideal without any power losses. The parameters of the motor circuit are as follows:

R_a = 0.289 Ω - phase resistance of the brushless DC motor

L_a = 0.002202H - phase inductance of the DC brushless motor

K_e = 6.85 *V/(rad/s)* - EMF constant.

J = 0.0092 kg/m^2 - moment of inertia

D = 0.0037 *Nm/(rad/s)*- friction coefficient

T_{load} = 350Nm - load torque

The motor's block diagram was constructed, as shown in fig 4.7a and fig 4.7b. Referring to Appendix-B, the following characteristics are observed after running the simulation:

- **Armature voltage (V_{ac}) and armature current (I_a) characteristics**

The Fig 4.7 shows the characteristics of armature voltage (V_a) and armature current (I_a) in dynamic condition. It can be observed from the waveforms that, though the voltage V_a is a square wave form, I_a has ripples because of commutation of currents in phases.

- **Source current(I_S) and load torque (T_L) characteristics**

The characteristics of source current (I_S) and load torque(T_L) can be seen from Fig 4.10. The Source current drops to zero as the load torque is applied and rises up steeply.

- **Electromagnetic torque (T_{em}), Speed (ω) and Load Torque (T_L) characteristics**

  The Fig 4.8 depicts the waveforms of electromagnetic torque (T_{em}), speed (ω) and load torque (T_L) in dynamic condition. It can be noted that the electromagnetic torque (T_{em}) rises steeply as the load torque is applied.

- **Characteristics of speed, efficiency, mechanical power and source current**

Fig 4.10 represents the steady state characteristics of RFTWTRPM motor operating as brushless dc motor. The efficiency is can be calculated using the following formula.

$$\text{Efficiency} = \frac{P_{out}}{P_{in}} \times 100 \tag{4.17}$$

Where P_{out} is output power

P_{in} is input power

By neglecting losses, in the present case

$$P_{out} = P_{em} = \omega \cdot T_{em} \tag{4.18}$$

Therefore the output power is dependent on speed and electromagnetic torque values. These effects can be observed in the Fig 4.10.

4.5 Performance of Brushless DC motor with Cogging Torque:

Looking at the distortion created by cogging torque, the SIMULINK block diagram in Fig 4.7a was created by neglecting the cogging torque. In present section, the speed torque characteristics of brushless DC motor (see Fig 4.12) in presence of cogging torque are to be simulated to observe the effect of cogging torque.

From the speed torque characteristics shown in Fig 4.11, severe distortions in the

waveforms of speed and torque were observed, which was due to the presence of cogging torque. Therefore during actual modeling of the motor, the cogging torque should be eliminated by process of skewing the slots.

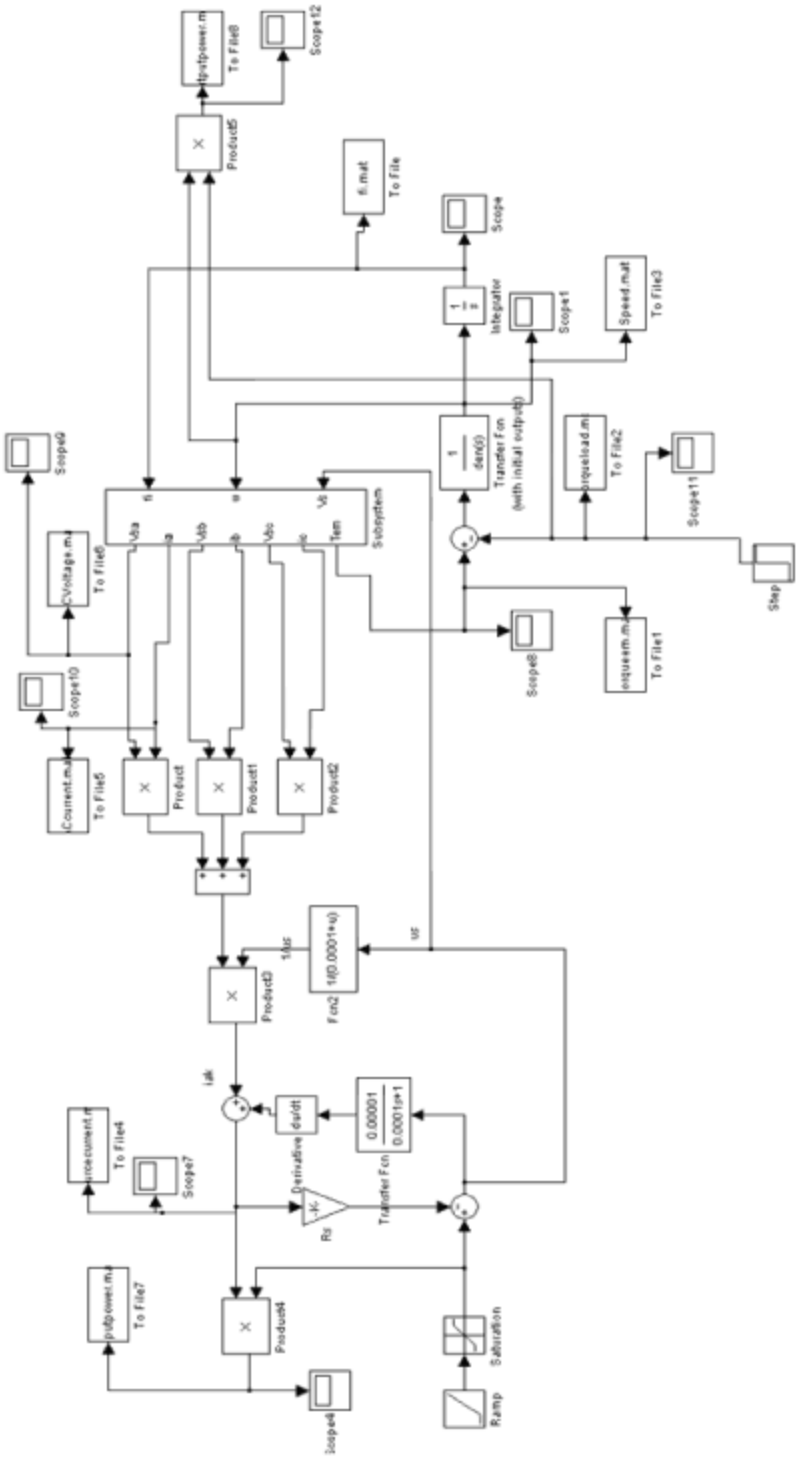

Fig. 4.6a SIMULINK block diagram of brushless DC motor

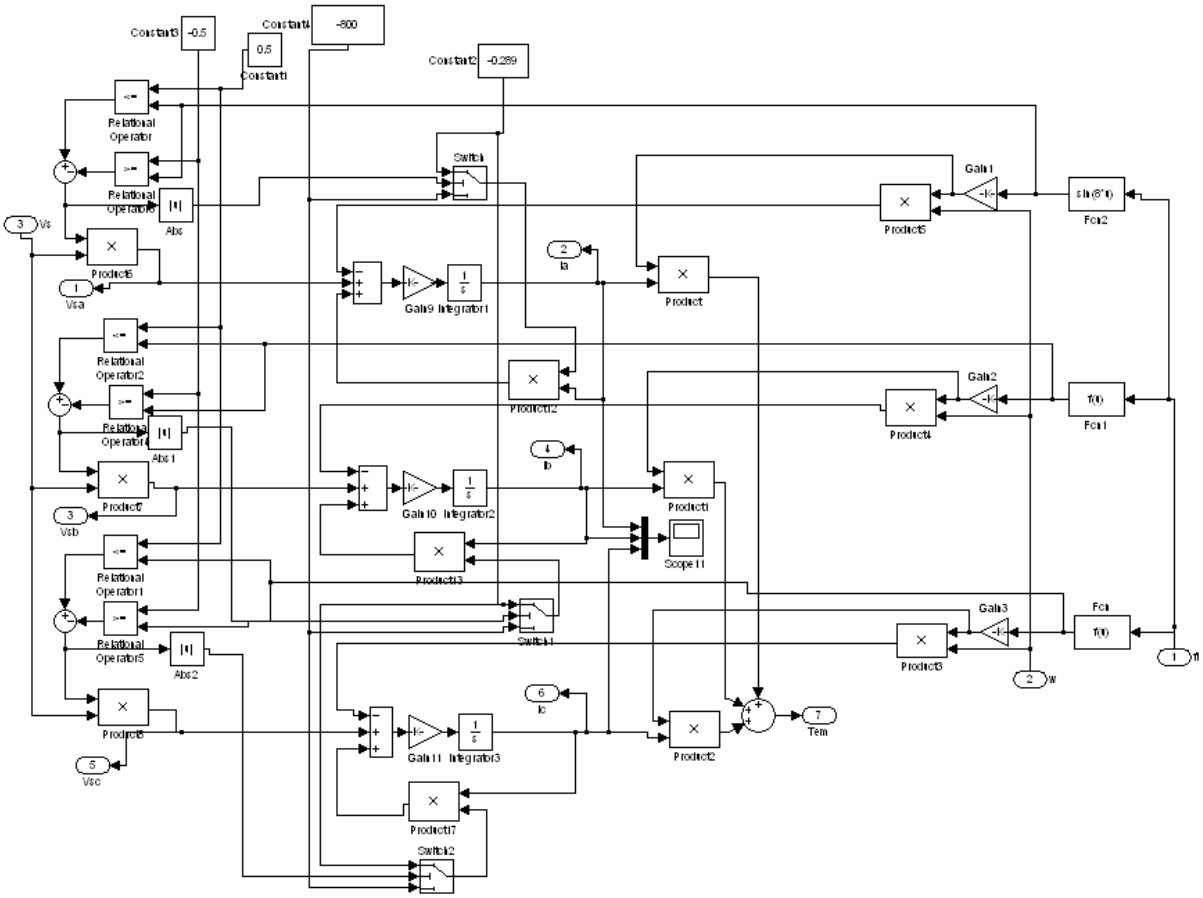

Fig. 4.6b SIMULINK block diagram of brushless DC motor subsystem

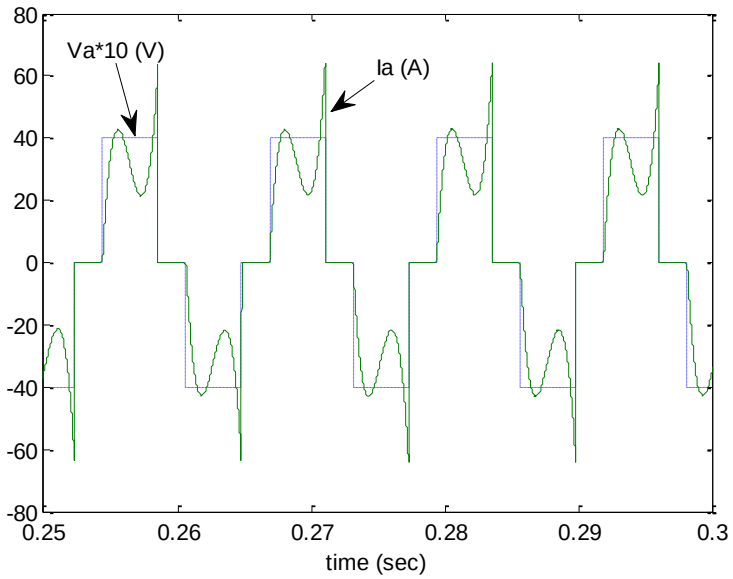

Fig 4.7 Phase voltage and phase current waveforms in steady state

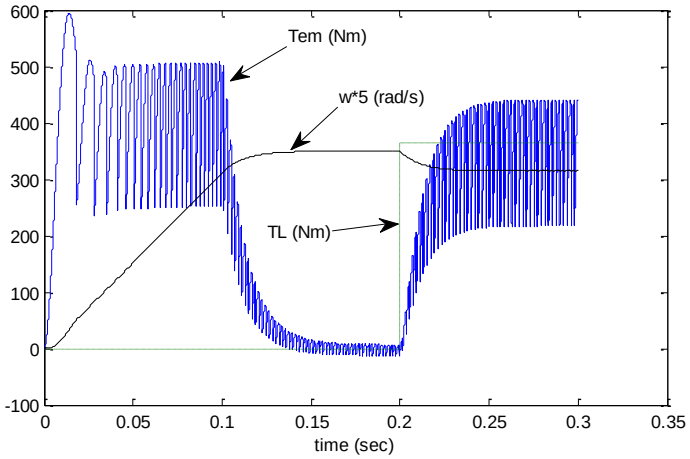

Fig 4.8 Dynamic characteristics of electromagnetic torque, speed and load torque vs. time

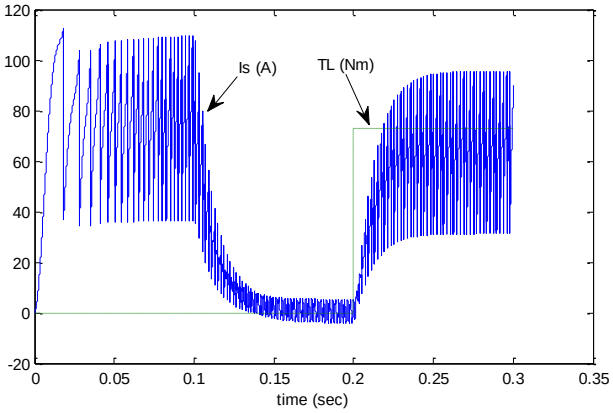

Fig 4.9 Dynamic characteristics of load torque and source current waveform

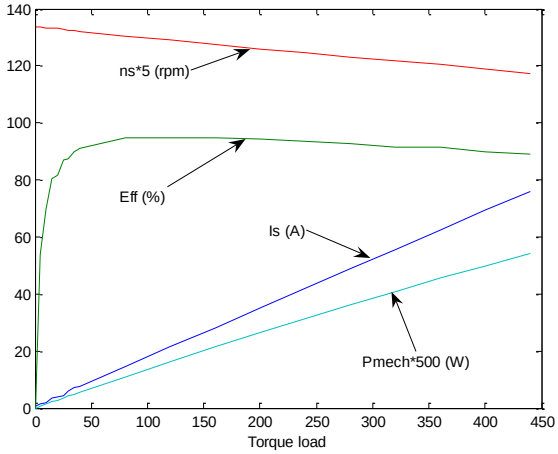

Fig 4.10 Electromechanical characteristics in steady state

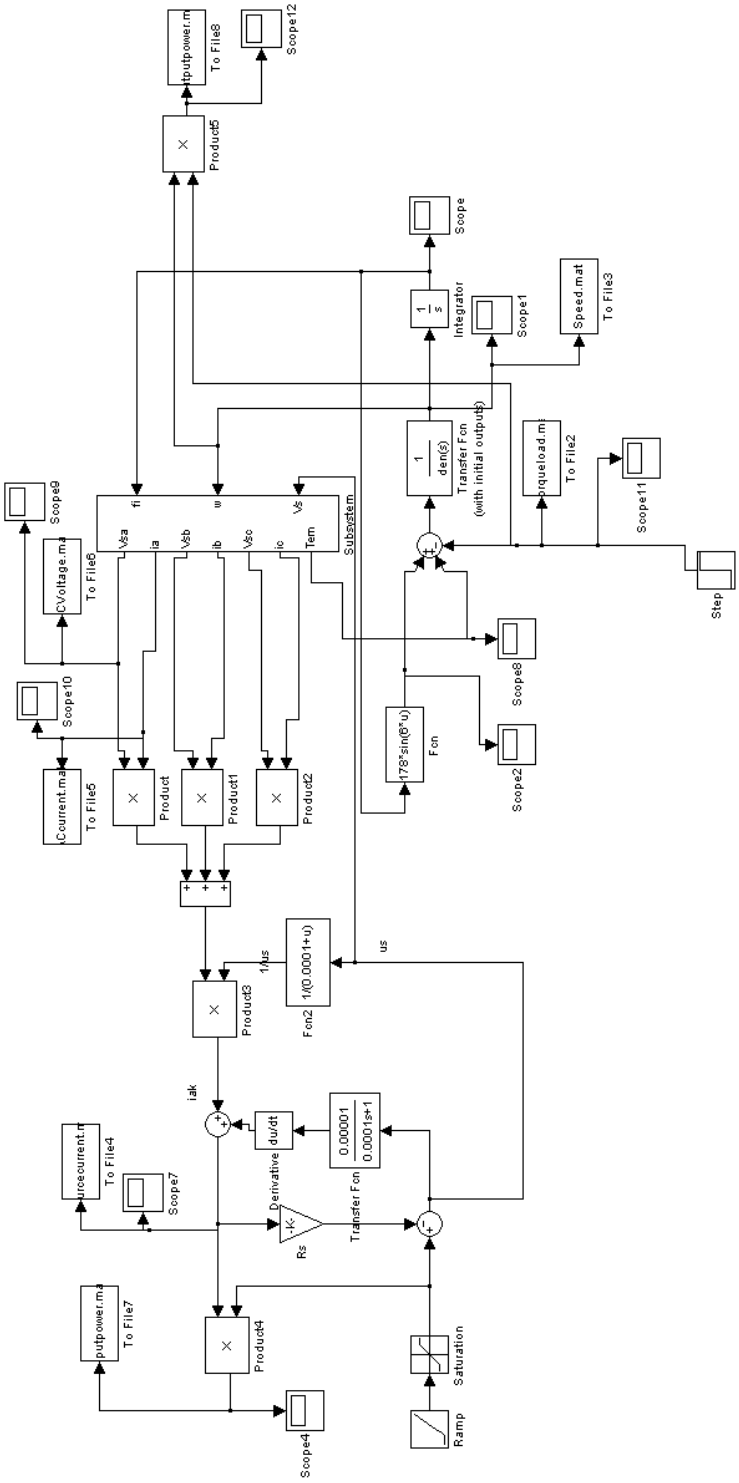

Fig 4.11 Block diagram of brushless DC motor with cogging torque

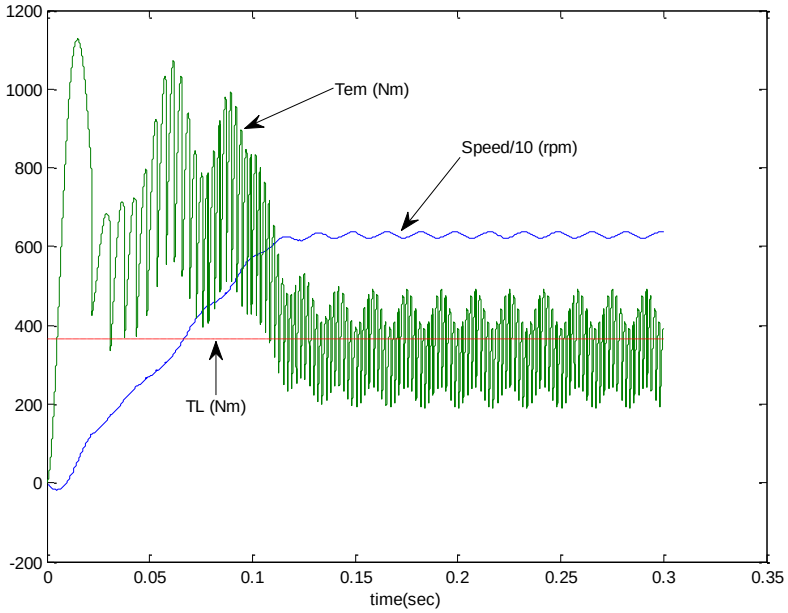

Fig 4.12 Speed torque characteristics

CHAPTER 5

CONCLUSIONS

The performance of RFTWTRPM motor was analyzed in this report. The analysis was carried out by using the dynamic model of the motor. The parameters for this model were determined from the FEM model simulation using 2-D FEMM program. The dynamic simulation was carried out using SIMULINK. The block diagram was developed from brushless DC motor operation. The following conclusions come out from the analysis.

- The RFTWTRPM motor with the winding placed in the slots develops greater torque than slotless motor model presented in [12]. This is due to higher magnetic flux density in the air gap.
- Unfortunately, the present version of RFTWTRPM motor with the toothed stator core introduced relatively high cogging torque. This torque does not reduce the average torque but introduces torque ripple in the torque waveform. In some applications of this motor like driving light vehicles, this torque ripple cannot be accepted.
- To reduce the cogging torque, the stator core length should be skewed. The analysis of the motor with the skewed teeth can be performed only using 3-D FEM simulation which was beyond the scope of this thesis.
- Though the RFTWTRPM motor is supplied from AC source, its electromechanical characteristics in steady state are similar to the ones of conventional brush DC motor.
- Referring to previous two conclusions, it can be stated that brushless DC motor offers similar electromechanical characteristics as brush DC motor with efficiency as high as 95%. Brushless DC motors need lower maintenance due to the lack of commutator.

REFERENCES

[1]. Ronghai Qu and Thomas A.Lipo, "Design and Parameter Effect Analysis of Dual-Rotor, Radial-Flux, Toroidally Wound, Permanent-Magnet Machines," IEEE TRANSACTIONS ON INDUSTRY APPLICATIONS, VOL. 40, NO. 3, MAY/JUNE 2004, pp.771-779.

[2]. Ronghai Qu and Thomas A.Lipo, "Dual-Rotor, Radial-Flux, Toroidally Wound, Permanent-Magnet Machines," IEEE TRANSACTIONS ON INDUSTRY APPLICATIONS, VOL. 39, NO. 6, NOVEMBER/DECEMBER 2003, pp. 1665-1673.

[3]. A. Di Napoli, F. Caricchi, F. Crescimbini and G. Noia, "Design criteria of a low-speed axial-flux PM synchronous machine" University of Rome "La Sapienza" – Electrical Engineering Dept.

[4]. F. Profumo, A. Tenconi, Z. Zhang, and A. Cavagnino, "Novel axial flux interior PM synchronous motor realized with powdered soft magnetic materials," in *Conf. Rec. IEEE-IAS Annu. Meeting*, vol. 1, St. Louis, MO, 1998, pp. 152–158.

[5]. J. Luo, S. Huang, S. Chen, and T. A. Lipo, "Design and experiments of a novel axial flux circumferential current permanent magnet (AFCC) machine with radial airgap," in *Conf. Rec. IEEE-IAS Annu. Meeting*, vol.2, Chicago, IL, 2001, pp. 1989–1996.

[6] M. Aydin, S. Huang and T. A. Lipo, "Design and electromagnetic field analysis of non-slotted and slotted TORUS type axial flux surface mounted disc machines", *IEEE International Conference on Electrical Machines and Drives*, Boston, 2001, pp.645-651.

[7] A.Kaddouri, H.Le-Huy, "Analysis and design of a slotless NDFEB permanent-magnet synchronous motor for direct drive," Industry Applications Society Annual Meeting, 1992., Conference Record of the 1992 IEEE, Vol.1, 4-9 Oct 1992, pp. 271-278.

[8] Ronghai Qu, Aydin.M and Thomas A.Lipo "Performance Comparison of Dual-Rotor Radial-Flux and Axial-Flux Permanent-Magnet BLDC Machines," Electric Machines and Drives Conference, 2003. IEMDC'03. IEEE International**,** Vol.3, 1-4 June 2003, pp. 1948- 1954.

[9] Ned Mohan, "Advanced Electric Drives: Analysis, Control and Modeling using Simulink", 2001 Edition.

[10] David Meeker, "Finite Element Method Magnetics – Version 4.0", User's Manual, January 8, 2006.

[11] Dr. Ernest Mendrela, Lecture notes on PM Synchronous Motor Design, Louisiana State University, Baton Rouge, LA.

[12] Pavani Gottipati, "Comparitive study of double-rotor permanent magnet brushless motors with cylindrical and disc type slot-less stator", Thesis document, Louisiana State University, Baton Rouge, August 2007.

[13] Deepthi Chikkam, "Performance of disc brushless DC motor applied as gearless drive for wheelchair", Thesis document, Louisiana State University, Baton Rouge, Dec 2005.

[14] Sophie Sekalala, “Performance of three-phase permanent magnet motor operating as a synchronous motor and brushless DC motor”, Thesis document, Louisiana State University, Baton Rouge, Aug 2006.

APPENDIX-A: TORQUE CHARACTERISTICS OF RFTWTRPM MOTOR

```
% Single-phase torque, three-phase torque, synchronous torque and cogging torque
characteristics for RFTWTRPM motor
theta_m = [0  0.5 1   1.5 2   2.5 3   3.5 4   4.5 5   5.5 6   6.5 7   7.5 8   8.5 9   9.5 10  10.5   11
11.25  11.5   12  12.5   13  13.5   14  14.5   15  15.5   16  16.5   16.875  17  17.5   18  18.5
18.75  19  19.5   20  20.5   21  21.5   22  22.5]
theta_m_i  = [0   5.6250   11.2500   16.8750   22.5000]
t_3ph = [-364.843 -366.628   -379.506   -162.662   -98.3862   -122.434   -188.17 -238.275   -
271.955   -314.022   -414.166   -457.889   -386.355   -237.005   -203.286   -192.78 -168.14 -
150.166   39.6669 132.946 110.537 44.608  8.08785 16.4011 14.3927 -30.7525   -112.33 -
135.384   -44.8736   123.029 196.582 187.953 205.251 215.144 394.652 477.95  450.706
414.816 337.65  270.026 264.861 264.568 195.336 118.564 79.5085 168.474 354.297 359.055
363.471]
t_3ph_i = [-364.843   -468.613   16.4011 477.95  363.471]
t_1ph = [-188.342 -193.71 -209.087   -0.963264   47.6392 10.3846 -69.2637   -133.75 -191.418
-249.923   -365.105   -418.941   -356.598   -213.924   -186.7  -184.742   -168.681   -157.147
31.0314 124.152 101.415 38.1381 4.9088  16.7666 17.6266 -24.402 -103.447   -125.812   -
36.0357   130.646 200.398 179.697 188.241 192.04  364.391 440.811 411.821 365.632 275.46
190.937 174.148 162.155 77.8056 -13.8287   -65.2244   6.40196 182.867 185.826 187.029]
t_1ph_i  = [-188.342  -431.377   16.7666 440.811 187.029]
t3diff  = [-365.006206 -357.26413  -357.4917   -338.4  -314.5342   -297.97 -282.4591   -
272.6776   -257.2995   -239.9537   -236.594   -229.869   -230.274   -228.91667  -209.78845  -
187.39497  -158.50359  -135.3701   -116.4781   -90.229 -68.412 -45.2936   -18.49255   -1.5322
13.525104   43.0705 68.694  88.263  119.0674   136.3502   148.7292   187.8692151 210.54183
229.5342   229.662 226.953 229.72  237.541 242.5703   253.5993   261.11589   270.71414
279.8986   296.495 309.9725   339.815 356.45189   358.01786   364.000587]
t1diff  = [-188.505206 -184.34613  -187.0727   -176.701264 -168.5088   -165.1514   -163.5528
-168.1526   -176.7625   -175.8547   -187.533   -190.921   -200.517   -205.83567  -193.20245  -
179.35697  -159.04459  -142.3511   -125.1136   -99.023 -77.534 -51.7635   -21.6716   -1.1667
16.759004   49.421  77.577  97.835  127.9053   143.9672   152.5452   179.6132151 193.53183
206.4302   199.401 189.814 190.835 188.357 180.3803   174.5103   170.40289   168.30114
162.3682   164.1023   165.2396   177.74296   185.02189   184.78886   187.558587]
t_cog  = [0.163206 -9.36387   -22.0143   175.738 216.148 175.536 94.2891 34.4026 -14.6555
-74.0683   -177.572   -228.02 -156.081   -8.08833   6.50245 -5.38503   -9.63641   -14.7959
156.145 223.175 178.949 89.9016 26.5804 17.9333 0.867596   -73.823 -181.024   -223.647   -
163.941   -13.3212   47.8528 0.0837849   -5.29083   -14.3902   164.99  250.997 220.986
177.275 95.0797 16.4267 3.74511 -6.14614   -84.5626   -177.931   -230.464   -171.341   -
2.15489   1.03714 -0.529587]
t_syn  = [-365.006206  -254.271   -134.359   -285.177   -492.576   -430.797   -365.194   -
283.353   -131.255   -278.594   -494.197   -434.594   -358.534   -281.913   -134.948   -
293.889   -489.906   -438.991   -364.227]
%3-ph Torque characteristics
figure(1),
plot(theta_m,t_3ph,theta_m,0,':',theta_m,t_cog,theta_m,0,'--
',theta_m_i,t_3ph_i,theta_m_i,0,':',theta_m,t3diff,theta_m,0,'--'),grid,
%1-ph Torque characteristics
```

```
figure(2),
plot(theta_m,t_1ph,theta_m,0,':',theta_m,t_cog,theta_m,0,'--
',theta_m_i,t_1ph_i,theta_m_i,0,':',theta_m,t1diff,theta_m,0,'--'),grid,
%Synchronous torque characteristics
figure(3),
plot(theta_m,t_syn,theta_m,0,':',theta_m,t_cog,theta_m,0,'--',theta_m,t_diff,theta_m,0,':'),grid,
```

APPENDIX B: PERFORMANCE CHARACTERISTICS OF RFTWTRPM MOTOR OPERATING AS BRUSHLESS DC MOTOR

```
% Performance characteristics of RFTWTRPM model operating as brushless DC motor
load Inputpower Pin;
load Outputpower Pout;
load Speed w;
load Torqueload TL;
load Torqueem;
load ACcurrent;
load Sourcecurrent Is;
load ACcurrent Iac;
load Torqueem Tem;
load ACvoltage Vac;
Pin=Pin'; Pout=Pout'; w=w'; TL=TL'; Iac=Iac';Is=Is';Tem=Tem';Vac=Vac';
t=w(:,1); Pin=Pin(:,2);w=w(:,2);TL=TL(:,2);Iac=Iac(:,2);Is=Is(:,2);Tem=Tem(:,2);Vac=Vac(:,2);
figure(1),
plot(t,Is,':',t,TL/5,':'),
xlabel('time t(sec)'),ylabel('Load Torque-TL(N-m),Source Current-Is(amp)');
figure(2),
plot(t,Tem,':',t,TL,':',t,w*5,':'),
xlabel('time t(sec)'), ylabel('Load Torque-TL(N-m),Electro-mag. torque-Tem(N-m), Speed-
W(rad/s)');
figure(3),
plot(t,Vac/10,':',t,Iac,':'),
xlabel('time t(sec)'), ylabel('ACVoltage-Vac (V),ACcurrent-Iac (amp)');
Pinm=mean(Pin);wm=mean(w);TLm=mean(TL);Ism=mean(Is);Temm=mean(Tem);
```

APPENDIX-C: PERFORMANCE CHARACTERISTICS OF RFTWTRPM MOTOR OPERATING AS BRUSHLESS DC MOTOR IN STEADY STATE

```
% Performance characteristics of RFTWTRPM model operating as brushless DC motor in steady state
TL=[0 90 180 270 365 450 540 630 720 810 900 990 1080 1170 1260 1350 1440 1530];
ns=[552.52 548.02 543.05 537.99 532.64 528.16 523.48 518.99 514.59 510.49 506.38 502.56 498.84 495.21 491.68 488.43 485.09 482.03];
Is=[24.49 28.68 33.01 37.42 42.08 46.25 50.65 55.06 59.49 63.95 68.39 72.82 77.18 81.59 85.95 90.43 95.01 99.29];
Pin=[5.78e3 7.51e3 9.26e3 1.10e4 1.29e4 1.45e4 1.63e4 1.81e4 1.98e4 2.16e4 2.39e4 2.52e4 2.69e4 2.87e4 3.04e4 3.22e4 3.4e4 3.57e4];
Pout=[0 2.15e3 4.23e3 6.20e3 8.16e3 9.83e3 1.15e4 1.31e4 1.47e4 1.61e4 1.75e4 1.88e4 2.01e4 2.12e4 2.23e4 2.34e4 2.45e4 2.54e4];
Eff=[0 28.63 45.68 56.36 63.26 67.79 70.55 72.38 74.24 74.53 73.22 74.60 74.72 73.86 73.35 72.67 72.05 71.15];
figure(1),
plot (TL,ns/10,':',TL,Is,':',TL,Pout/100,':',TL,Eff,':'),
xlabel('Torque Load-TL(N-m)');
```

VITA

Ravi Kishore Pratapa was born in January, 1984, in Visakhapatnam City, Andhra Pradesh, India. He finished his undergraduate studies at Anna University in April 2005. In August 2006 he came to Louisiana State University to pursue graduate studies in electrical engineering. He is currently a candidate for the degree of Master of Science in Electrical Engineering, which will be awarded in May 2010.